

# **Optical Path Length Multiplexing of Optical Fiber Sensors**

by

Thomas A. Wavering

Thesis submitted to the Faculty of the  
Virginia Polytechnic Institute and State University  
in partial fulfillment of the requirements for the degree of

**MASTER OF SCIENCE**

in

Electrical Engineering

## **APPROVED:**

Richard O. Claus, Chairman

Kent A. Murphy

Gary S. Brown

February, 1998

Blacksburg, Virginia

**Keywords:** Optical fiber sensors, interferometry, extrinsic Fabry-Perot interferometer, sensor multiplexing

Copyright 1998, Thomas A. Wavering

# Optical Path Length Multiplexing of Optical Fiber Sensors

by

Thomas A. Wavering

Richard O. Claus, Chairman

Electrical Engineering

## Abstract

Optical fiber sensor multiplexing reduces cost per sensor by designing a system that minimizes the expensive system components (sources, spectrometers, etc.) needed for a set number of sensors. The market for multiplexed optical sensors is growing as fiber-optic sensors are finding application in automated factories, mines, offshore platforms, air, sea, land, and space vehicles, energy distribution systems, medical patient surveillance systems, etc. Optical path length multiplexing (OPLM) is a modification to traditional white-light interferometry techniques to multiplex extrinsic Fabry-Perot interferometers and optical path length two-mode sensors. Additionally, OPLM techniques can be used to design an optical fiber sensor to detect pressure/force/acceleration and temperature simultaneously at a single point. While power losses and operating range restrictions limit the broadscale applicability of OPLM, it provides a way to easily double or quadruple the number of sensors by modifying the demodulation algorithm. The exciting aspect of OPLM is that no additional hardware is needed to multiplex a few sensors. In this way OPLM works with conventional technology and algorithms to drastically increase their efficiency. [1]

## **Acknowledgments**

I would like to thank my committee members for their encouragement and guidance throughout my studies at Virginia Tech. I would like to thank Dr. Kent Murphy for introducing me to the world of fiber optics in my senior level fiber optics class and for responding to my emails and phone calls for an assistantship with a GRA position at the Fiber and Electro-Optics Research Center. I must also thank Dr. Gary Brown for making me enjoy electromagnetics and recognizing the constant presence of rough surface scattering. Finally, I must thank Dr. Richard Claus for all of his guidance, support, and encouragement throughout my graduate studies.

I enjoyed working with FEORC, even though most of my time was spent with F&S. Thanks to all at F&S who helped in my research, especially Scott Meller who helped guide my research, shoot down my crazy ideas, and explain my even crazier ideas.

I thank my parents, my family, and my girlfriend, Liz, for their faith, encouragement, love, wisdom, and example. They have taught me countless truths and instilled in me values and vigor with which I try to live my life. From when I used to draw satellites in elementary school and convince my dad to take them into work for his company to use, my parents have encouraged and challenged me to be the best person I can be, and I thank them.

I would like to acknowledge the partial support of this research and my education provided by the multiple contracts I worked on at both FEORC and F&S: an Air Force AASERT Program to develop multiplexed thermally compensated optical fiber pressure sensors and a NASA Phase I SBIR, "Micromachined Fiber Optic Accelerometers" out of Dryden Flight Research Center. Thanks to these organizations for their support of this research.

## Table of Contents

<b>1. Chapter 1 - Introduction</b>	<b>1</b>
<b>1.1 Optical Fiber Sensors</b>	<b>1</b>
<b>1.2 Extrinsic Fabry-Perot Interferometer</b>	<b>2</b>
1.2.1 Theory of Operation	3
1.2.2 Two beam approximation	4
1.2.3 Sensor Applications	7
1.2.4 Demodulation Techniques	13
<b>1.3 Overview</b>	<b>16</b>
<b>2. Chapter 2 - Optical Fiber Sensor Multiplexing</b>	<b>17</b>
<b>2.1 Multiplexing Topologies</b>	<b>17</b>
<b>2.2 Current Multiplexing Technologies</b>	<b>19</b>
2.2.1 Spatial Multiplexing	20
2.2.2 Time Division Multiplexing	20
2.2.3 Wavelength Division Multiplexing	21
2.2.4 Frequency Division Multiplexing	21
<b>2.3 Optical Path Length Multiplexing</b>	<b>22</b>
2.3.1 Use of Optical Path Length Multiplexing with other Multiplexing Techniques	22
<b>3. Chapter 3 - Optical Path Length Multiplexing</b>	<b>24</b>
<b>3.1 Theory</b>	<b>24</b>
<b>3.2 Tests to find minimal buffer zone</b>	<b>26</b>
<b>3.3 Tests for double gap</b>	<b>29</b>
<b>3.4 Theoretical limits of operation</b>	<b>31</b>
<b>3.5 Verification of Optical Path Length Multiplexing</b>	<b>32</b>

<b>4. Chapter 4 - Applications of Optical Path Length Multiplexing</b>	<b>35</b>
<b>4.1 Multiplexed Extrinsic Fabry-Perot Interferometers</b>	<b>35</b>
<b>4.2 Multiplexed Two-mode Sensors</b>	<b>38</b>
<b>4.3 Hybrid Temperature and Pressure Sensor</b>	<b>41</b>
<b>4.4 Low-profile Extrinsic Fabry-Perot Interferometers</b>	<b>43</b>
<b>5. Chapter 5 - Conclusions and Future Work</b>	<b>45</b>
<b>5.1 Conclusion</b>	<b>45</b>
<b>5.2 Future Work</b>	<b>45</b>

## List of Illustrations

<i>Figure 1-1. Extrinsic Fabry-Perot Interferometer.</i>	3
<i>Figure 1-2. Fringe output of Extrinsic Fabry-Perot Interferometer.</i>	4
<i>Figure 1-3. Low finesse Fabry-Perot output and two beam approximation.</i>	5
<i>Figure 1-4. EFPI output with sensing reflection coupling loss.</i>	6
<i>Figure 1-5. EFPI strain sensor.</i>	8
<i>Figure 1-6. EFPI strain sensor vs. conventional strain gauge.</i>	8
<i>Figure 1-7. EFPI accelerometer design.</i>	9
<i>Figure 1-8. Demonstration of EFPI accelerometer.</i>	10
<i>Figure 1-9. EFPI pressure sensor design.</i>	11
<i>Figure 1-10. Demonstration of EFPI pressure sensor.</i>	11
<i>Figure 1-11. EFPI temperature sensor design.</i>	12
<i>Figure 1-12. Low-profile EFPI design.</i>	13
<i>Figure 1-13. Intensity-based EFPI output transfer function.</i>	14
<i>Figure 1-14. White-light interferometric demodulation setup.</i>	15
<i>Figure 1-15. EFPI interferometric output for a gap of 50.45mm.</i>	15
<i>Figure 2-1. Serial multiplexing topologies.</i>	18
<i>Figure 2-2. Spatial multiplexing topologies.</i>	18
<i>Figure 2-3. Hybrid spatial multiplexing and optical path length multiplexing system.</i>	23
<i>Figure 3-1. EFPI interferometric output for two multiplexed sensors.</i>	25
<i>Figure 3-2. Power spectral density for two multiplexed sensors.</i>	25
<i>Figure 3-3. Buffer zone testing setup.</i>	26
<i>Figure 3-4. Variable gap EFPI setup.</i>	27
<i>Figure 3-5. a) Returned wave spectrum from two multiplexed EFPIs. b) Power spectral density showing two EFPI sensor peaks at 50mm.</i>	27
<i>Figure 3-6 a) Returned wave spectrum from two multiplexed EFPIs. b) Power spectral density showing one EFPI sensor peak at 50mm and another smaller peak around 65mm.</i>	28

<i>Figure 3-7. a) Returned wave spectrum from two multiplexed EFPIs. b) Demodulated wave spectrum showing one EFPI sensor peak at 50mm and another smaller peak around 80mm.</i>	29
<i>Figure 3-8. EFPI Sensor with highly reflective reflector to generate double gap effect.</i>	29
<i>Figure 3-9. Test for double gap.</i>	30
<i>Figure 3-10. a) Returned wave spectrum from two multiplexed EFPIs both with 50mm gaps. b) Demodulated wave spectrum showing one EFPI sensor peak around 50um.</i>	31
<i>Figure 3-11. Spectrum of variable gap EFPI at 918 mm.</i>	32
<i>Figure 3-12. Optical path length multiplexing verification test setup.</i>	32
<i>Figure 3-13. Spectrums of two multiplexed EFPIs at three different strains.</i>	33
<i>Figure 3-14. Power spectral densities of two multiplexed EFPIs at three different strains.</i>	34
<i>Figure 3-15. Two multiplexed EFPIs and a foil strain gauge</i>	34
<i>Figure 4-1. Three serially multiplexed EFPIs.</i>	36
<i>Figure 4-2. Multiplexed EFPI spectrum.</i>	36
<i>Figure 4-3. Multiplexed EFPI power spectrum.</i>	36
<i>Figure 4-4. Multiplexed EFPI operation.</i>	37
<i>Figure 4-5. Two-mode force sensor results.</i>	38
<i>Figure 4-6. Two-mode temperature sensor.</i>	39
<i>Figure 4-7. Spectrum of a multiplexed EFPI and a two-mode sensor.</i>	39
<i>Figure 4-8. Power spectral density of multiplexed EFPI and two-mode sensor.</i>	40
<i>Figure 4-9. EFPI and two-mode sensors.</i>	40
<i>Figure 4-10. Hybrid temperature/pressure sensor design.</i>	41
<i>Figure 4-11. a) Returned wave spectrum from the pressure transducer. b) Demodulated spectrum showing the three signals detected: the air gap, the glass thickness, and the combination of the two.</i>	42
<i>Figure 4-12. Temperature detection with sensor diaphragm.</i>	43
<i>Figure 4-13. Low-profile multiplexing design.</i>	44

*Figure 5-1. Thermally compensated pressure sensor system design.* \_\_\_\_\_ 46  
*Figure 5-2. Multiplexed pressure sensor system design.* \_\_\_\_\_ 46

## **1. Chapter 1 - Introduction**

The motivation behind optical fiber sensor multiplexing is to reduce sensor cost by designing a system that minimizes the number of expensive system components (sources, spectrometers, etc.) needed for a given number of sensors. The market for multiplexed optical sensors is growing as fiber-optic sensors are finding application in automated factories, mines, offshore platforms, air, sea, land, and space vehicles, energy distribution systems, medical patient surveillance systems, etc. Optical path length multiplexing (OPLM) is a modification of traditional white-light interferometry techniques that is used to multiplex extrinsic Fabry-Perot interferometers (EFPIs), intrinsic Fabry-Perot interferometers (IFPIs), as well as interferometric two-mode sensors. While power losses and operating range restrictions limit its large-scale applicability, OPLM provides a way to easily double or quadruple the number of sensors by modifying the demodulation algorithm. [1]

### ***1.1 Optical Fiber Sensors***

Optical fiber sensors have several advantages over conventional sensing technologies. They have the advantages of small size, light weight, high sensitivity, high temperature capabilities, immunity to electromagnetic interference, and potential for large-scale multiplexing. The increased use of optical fiber components in telecommunications networks has resulted in mass production of several electrical and optical components which can be used in optical fiber sensor systems as well. This increased component availability has contributed to reduced optical sensor system costs. [2]

Optical fiber sensors have found numerous applications in industry. One of the largest commercial markets is for optical fiber gyroscopes, especially those used in automotive navigation systems. Additionally, optical fiber sensors have found application as strain sensors for smart structures, high temperature pressure sensors, ultra-sensitive accelerometers, and several other sensor applications. Optical fiber sensors are also finding increased use in biological, chemical, and magnetic field applications.

Optical fiber sensors operate as either as intrinsic or extrinsic sensors. In intrinsic sensors, an external measurand induces a change in the wave guiding properties of the medium. Intrinsic sensors can be configured as either reflective or transmissive. In extrinsic sensors, the optical signal interacts with the external measurand which modulates it. Extrinsic sensors are generally reflective based. Sensor information is encoded by polarization effects, phase change, frequency modulation, wavelength shift, intensity modulation, etc. [3]

Optical fiber sensors also work on different operating principles. Some sensors are based on the interference between light waves, sensors of this type are referred to as interferometric. Fabry-Perot, Mach-Zehnder, Michelson, and Sagnac are different geometries of interferometric sensors. Other sensors are based on the loss of light from the fiber or coupled to the fiber and are referred to as intensity-based sensors.

### ***1.2 Extrinsic Fabry-Perot Interferometer***

The extrinsic Fabry-Perot interferometer (EFPI) is an optical fiber sensor based on the combination of two light waves. As seen in Figure 1-1, the EFPI consists of a single-mode source and a reflector fiber aligned by a hollow core silica tube.

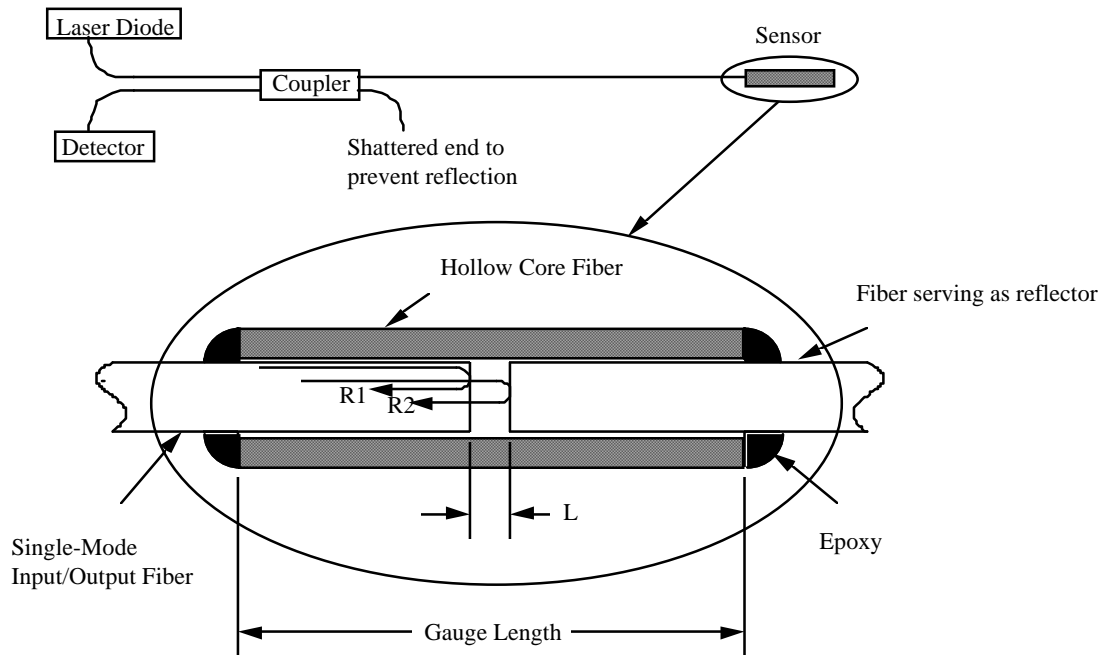


**Figure 1-1. Extrinsic Fabry-Perot Interferometer.**

### 1.2.1 Theory of Operation

The operation of an EFPI can be approximated as a two beam interferometer. When the laser diode light arrives at the source fiber end-face, a portion is reflected off the fiber/air interface (R1) and the remaining light propagates through the air gap (L) with a second reflection occurring at the air/fiber interface (R2). In an interferometric sense, R1 is the reference reflection and R2 is the sensing reflection. These reflective signals interfere constructively or destructively based on the optical path length difference between the reference and sensing fibers. The second output of the coupler is shattered to prevent reflections from interfering with the EFPI signal. Small movements in the hollow core cause a change in the gap length, which changes the phase difference between the sensing and reflecting waves producing fringes. [4]

If  $A_1$  and  $A_2$  are the amplitudes of the two waves and  $\Delta\phi$  is the phase difference between them, the intensity at the detector is given by

$$I_r = |A_1 + A_2|^2 = A_1^2 + A_2^2 + 2A_1A_2 \cos \Delta\phi \quad (1-1)$$

A typical output of the EFPI sensor is shown in Figure 1-2. A phase change of 360 degrees between the reflection and the reference corresponds to one fringe period. At a wavelength of  $1.3 \mu\text{m}$ , the change in gap for one fringe period is  $0.65 \mu\text{m}$ . As the reflector moves away from the source single mode fiber, the detector intensity drops due to a decrease in coupled power.

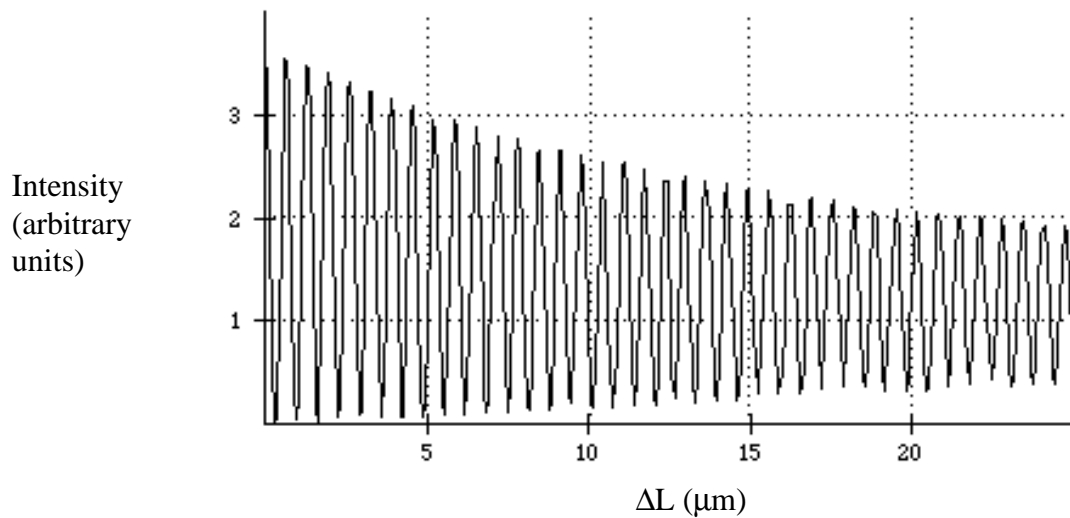


**Figure 1-2. Fringe output of Extrinsic Fabry-Perot Interferometer.**

### 1.2.2 Two beam approximation

Ideally, the EFPI is a two beam interferometer whose output is given by Equation 1-1.

The normalized received intensity of a Fabry-Perot cavity in reflection is [5]

$$I_r = \frac{1 - \cos \Delta\phi}{1 + R^2 - 2R\cos \Delta\phi} \quad (1-2)$$

where R is the power reflectivity of the interfaces between glass and air. In a two beam approximation of an EFPI, the denominator is taken to be one since R is small ( $\sim 0.035$ ) for a low finesse cavity (such as fused silica reflector), and the output becomes

$$I_r \approx 1 - \cos \Delta\phi \quad (1-3)$$

This approximation introduces some error in phase determination which is used to determine the change in gap by

$$\Delta\phi = \frac{4\pi\Delta L}{\lambda} \quad (1-4)$$

Equations (1-3) and (1-4) are plotted for different values of  $\Delta\phi$  in Figure 1-3. The maximum error induced in phase determination occurs when  $\Delta\phi = 2(m+1/2)\pi$ , m being an integer. The maximum error is 6.5% for  $R = 0.035$  [5]. The minimum error occurs at intervals of  $\pi/2$  at the quadrature point.

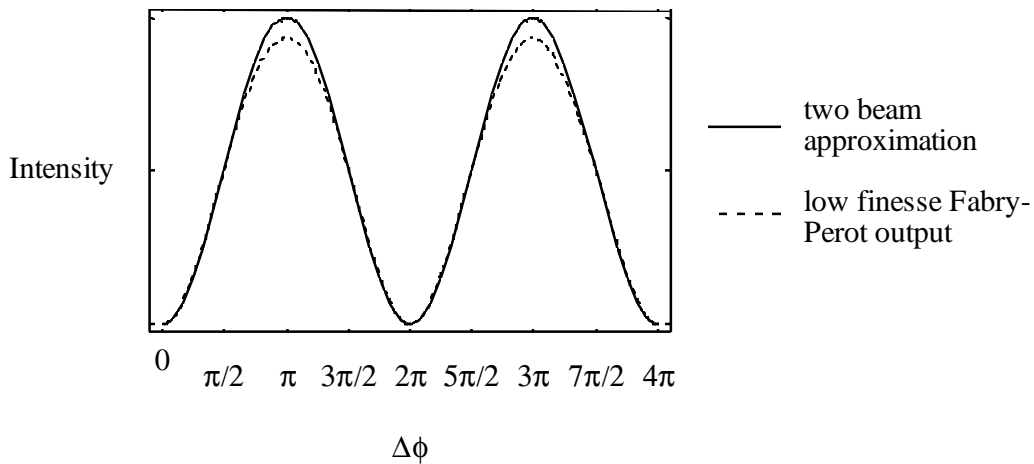


**Figure 1-3. Low finesse Fabry-Perot output and two beam approximation.**

The EFPI also deviates from an ideal two beam approximation because of the decrease in coupled power from the sensing reflection. The decrease in coupled power can be approximated in Equation 1-1 by redefining  $A_2$  using a simplified loss relation as [6]

$$A_2 = A_1 \left\{ \frac{ta}{a + 2L \tan[\sin^{-1}(NA)]} \right\}, \quad (1-5)$$

where  $a$  is the fiber core radius,  $L$  is the gap,  $t$  is the transmission coefficient of the air glass interface, and  $NA$  is the numerical aperture given by

$$NA = (n_1^2 - n_2^2)^{1/2}, \quad (1-6)$$

and  $n_1, n_2$  are the core and cladding refractive indexes respectively. Substituting Equation 1-5 into Equation 1-1 yields

$$I_r = A_1^2 \left( 1 + \left\{ \frac{ta}{a + 2L \tan[\sin^{-1}(NA)]} \right\}^2 + \frac{2ta}{a + 2L \tan[\sin^{-1}(NA)]} \cos(\Delta\phi) \right). \quad (1-7)$$

Equation 1-7 is plotted in Figure 1-4. From this plot it can be seen that as the gap increases, the sensitivity and signal to noise ratio also decrease. A measure of the available signal is the fringe visibility which is defined as

$$V = \frac{I_{\max} - I_{\min}}{I_{\max} + I_{\min}}. \quad (1-8)$$

As the gap increases, the fringe visibility decreases [4].

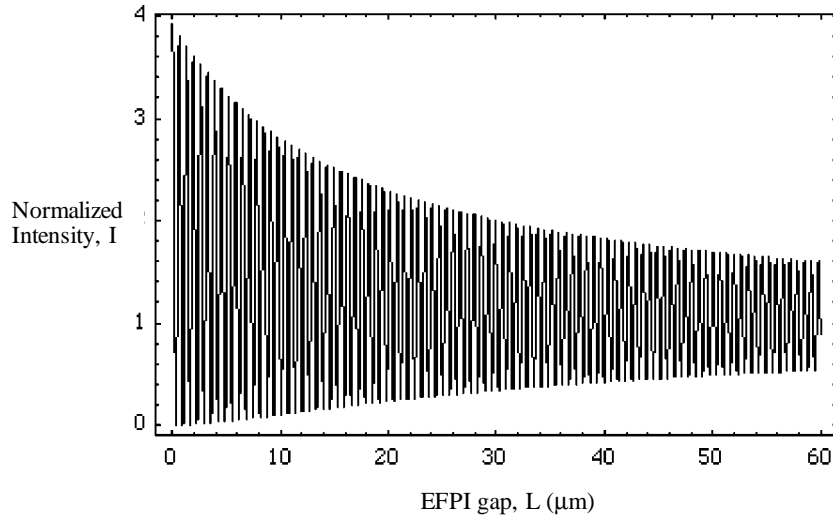


**Figure 1-4. EFPI output with sensing reflection coupling loss.**

In summary, the EFPI signal must be maintained around the quadrature point in order to obtain accurate information about the gap. If the particular sensing application demands a large dynamic range of operation, then the EFPI output will scan through multiple fringes and complex fringe counting methods must be employed [7]. For a large dynamic range, other techniques such as intensity demodulation or white-light interferometry must be used.

### 1.2.3 Sensor Applications

The extrinsic Fabry-Perot interferometer has several practical sensor applications. In each of these applications, the EFPI-based sensors were interrogated with an 830nm SLED source and demodulated with white-light interferometry techniques.

#### 1.2.3.1 Strain

For several years, EFPIs have been demonstrated as highly accurate strain gauges [8]. Figure 1-5 depicts one type of EFPI strain sensor construction. Strain is measured by dividing the relative change in gap ( $S$ ), by the gauge length of the sensor. This type of strain sensor is ideal for embedding within composite materials for structural health monitoring and smart structure applications. Figure 1-6 shows the output of two embedment type EFPI strain gages compared with a conventional foil strain gage surface attached. Because of the cylindrical shape of the EFPI sensor, epoxy was flooded over the sensor to guarantee efficient strain transfer between the beam and the sensor.

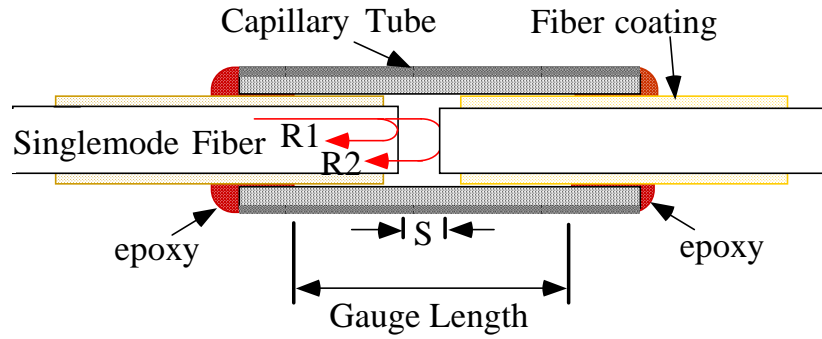


**Figure 1-5. EFPI strain sensor.**

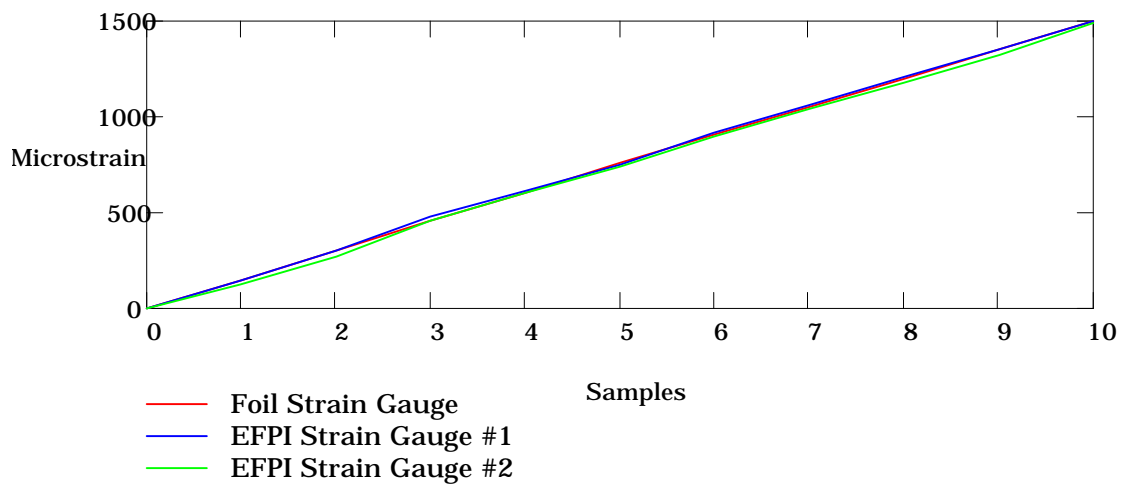


**Figure 1-6. EFPI strain sensor vs. conventional strain gauge.**

### 1.2.3.2 Accelerometer / Pressure Sensors

Extrinsic Fabry-Perot Interferometers can also be used as accelerometers and pressure sensors. Optical fibers sensors have several advantages over conventional sensors. EFPI sensors require no internal electronics, leading to a larger operating temperature range (with commercially available metal coated fiber, the upper temperature range is 750°C, and up to 2000°C with sapphire optical fiber). Additionally, EFPI sensors are immune to

electromagnetic interference and require no external electrical power which allows safe operation in combustible environments.

Figure 1-7 shows one configuration for an EFPI-type accelerometer. In this configuration, a silicon micromachined diaphragm with a small mass attached, is bonded to a pyrex housing which is epoxied to the single mode optical fiber. The diaphragm moves with the acceleration of the sensor. Circular diaphragm movement with acceleration is given by equation 1-9 [9]. In this equation,  $a$  = acceleration,  $y$  = deflection,  $h$  = thickness,  $E$  = Young's Modulus,  $m$  = mass,  $A$  = area,  $r$  = radius, and  $\mu$  = Poisson's Ratio.

$$a := \frac{A \cdot E \cdot h^4}{m \cdot r^4} \cdot \left[ \frac{16 \cdot y}{3 \cdot h \cdot (1 - \mu^2)} + \frac{y^3 \cdot (7 - \mu)}{h^3 \cdot 3 \cdot (1 - \mu)} \right] \quad (1-9)$$

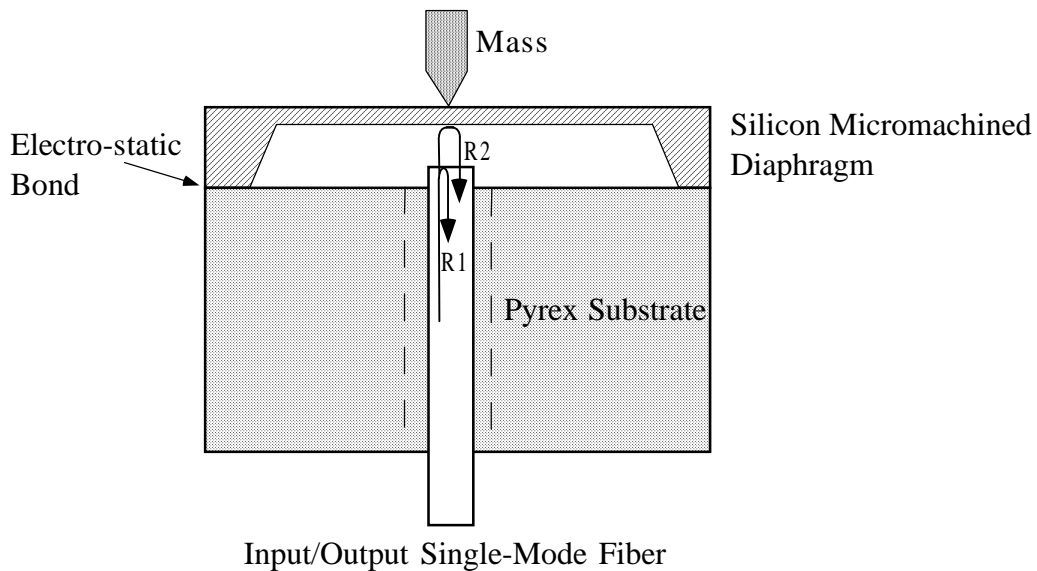


**Figure 1-7. EFPI accelerometer design.**

In an EFPI-type accelerometer, the diaphragm acts as the "reflecting fiber". Figure 1-8 shows the output of an EFPI accelerometer against a conventional accelerometer. The

optical fiber accelerometer tracks the conventional accelerometer quite well. The only noticeable difference is a slight lag in the response of the EFPI accelerometer.

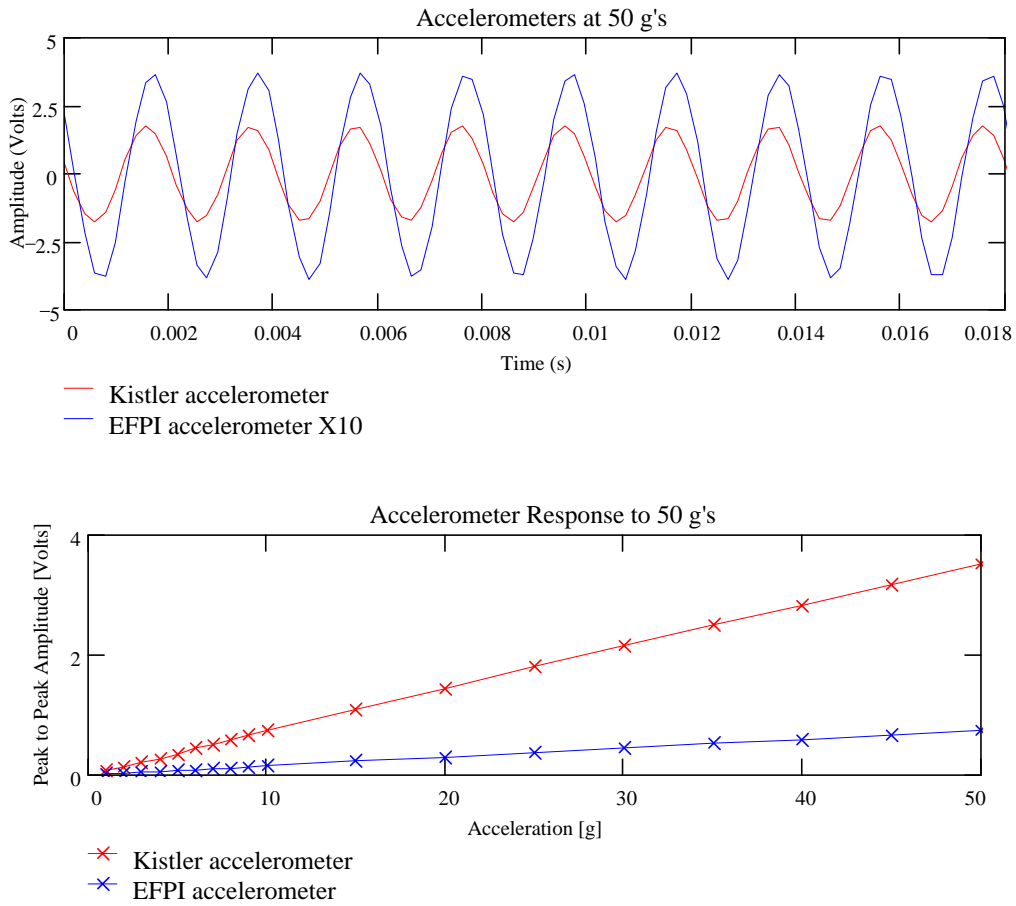


**Figure 1-8. Demonstration of EFPI accelerometer.**

Figure 1-9 depicts an EFPI-type optical fiber pressure sensor. In general, an EFPI-type pressure sensor is similar in construction to optical accelerometers, without the mass centered on the diaphragm. Figure 1-10 shows the results of testing of a crude 50 $\mu$ m diaphragm glass pressure transducer at two different temperatures. At the higher temperature, there is clearly a slight shift in the offset of the sensor. This offset can be corrected with thermal compensation.

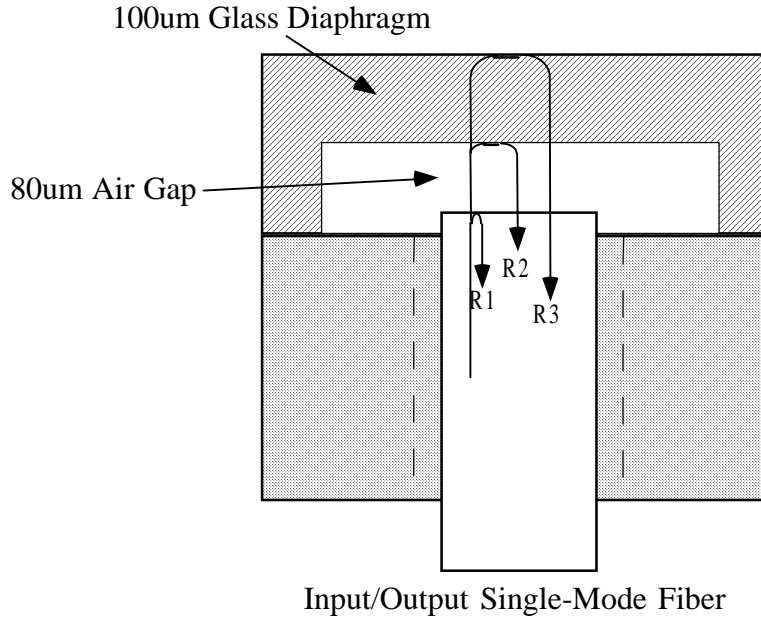


**Figure 1-9. EFPI pressure sensor design.**

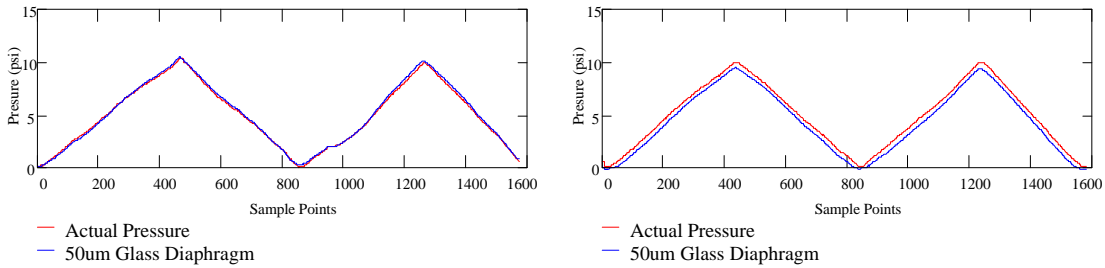


**Figure 1-10. Demonstration of EFPI pressure sensor at a) 26 °C and b) 45 °C.**

### 1.2.3.3 Temperature/Magnetic Field Sensor

The EFPI can also be used as a temperature or magnetic field sensor (Figure 1-11). As a temperature sensor, the reflecting fiber of the EFPI is replaced by a polished metal shaft. This metal shaft has a relatively high-CTE which results in a significant change in gap over temperature. An EFPI can also be used for a magnetic field sensor [10] by replacing the metal shaft with a magnetostrictive shaft (such as MetGlas). MetGlas changes length

with applied magnetic field. This change in length corresponds in a change in gap which can then be calibrated to a change in magnetic field.

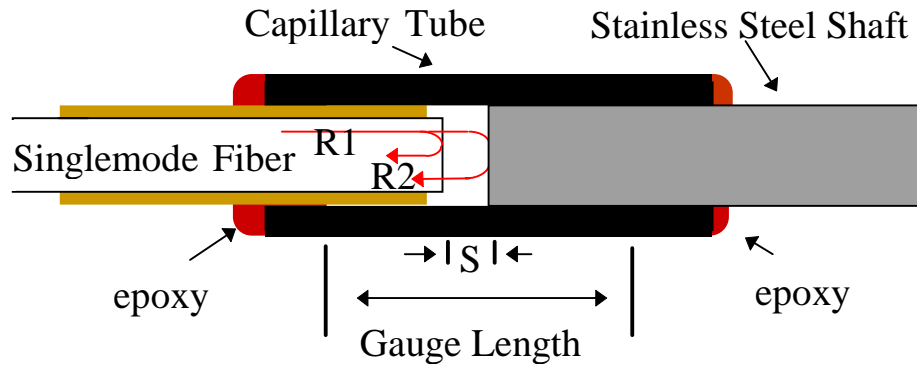


**Figure 1-11. EFPI temperature sensor design.**

#### 1.2.3.4 Low-profile sensor

Low-profile sensors have numerous applications in several different fields. Any diaphragm-based sensor mentioned above, can be redesigned as a low-profile EFPI sensor. One type of low-profile EFPI sensor utilizes an optical fiber polished at  $45^\circ$  to reflect the light. Another type of low-profile EFPI utilizes dielectric coatings to reflect a percentage of the light and transmit the rest [11]. In a low-profile EFPI sensor (Figure 1-12), the interferometric reflections are caused by R1, which reflects off of the optical fiber - air boundary, and a second reflection R2 off of the diaphragm. In this way a low-profile EFPI performs similar to a conventional EFPI, while maintaining a significantly lower profile. A low-profile design is useful for measuring acceleration, force, pressure, etc. against a surface without requiring orthogonal sensor leads.

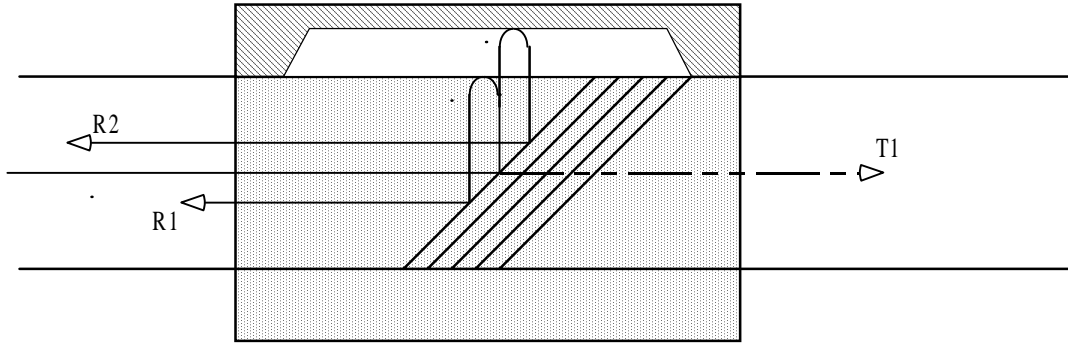


**Figure 1-12. Low-profile EFPI design.**

#### 1.2.4 Demodulation Techniques

There exist several different methods interrogate Extrinsic Fabry-Perot Interferometers. One method as explained in section 1.2.1, involves a fairly narrow bandwidth source. As the EFPI gap changes, the output intensity goes through fringes (Figure 1-2). For a 1300nm source, each fringe is about 0.63  $\mu\text{m}$ . Counting these fringes is one way to track EFPI gap changes. Because this method is interferometric rather than intensity-based it is insensitive to minor loss in the optical path. However this approach has two main concerns. The fringe characteristic of the sensor results in directional ambiguities in dynamic applications. Additionally, fringe counting cannot be used to provide absolute gap measurement. To resolve these concerns, two other demodulation approaches are often pursued.

##### 1.2.4.1 Intensity-based

In an intensity-based demodulation scheme, an LED source illuminates an EFPI sensor and a photodiode converts the optical signal into an electrical one. Figure 1-13 shows the change in intensity at the photodiode as the gap of an EFPI is changed from 0 to 200  $\mu\text{m}$ . This curve, unlike Figure 1-2, does not have any fringes because the coherence length of the broadband LED source is greater than the coherence length of the cavity, thus no

fringes appear. For a given sensor, this characteristic curve can be generated, thus enabling a high speed demodulation system. One problem with this method however, is that it relies on an EFPI returning the same intensity light for the same gap each time. Therefore, any loss (microbend, connector, splice, etc.) adds significant error into the system. Additionally, over temperature, the reflectivity of some materials changes. To get a strong intensity signal back at the photodiode, chromium or gold coated fibers are used as the reflecting fiber. However, as the temperature increases, the reflectivity of these mirrors changes. Other materials, such as platinum are being investigated for use in higher temperature applications.

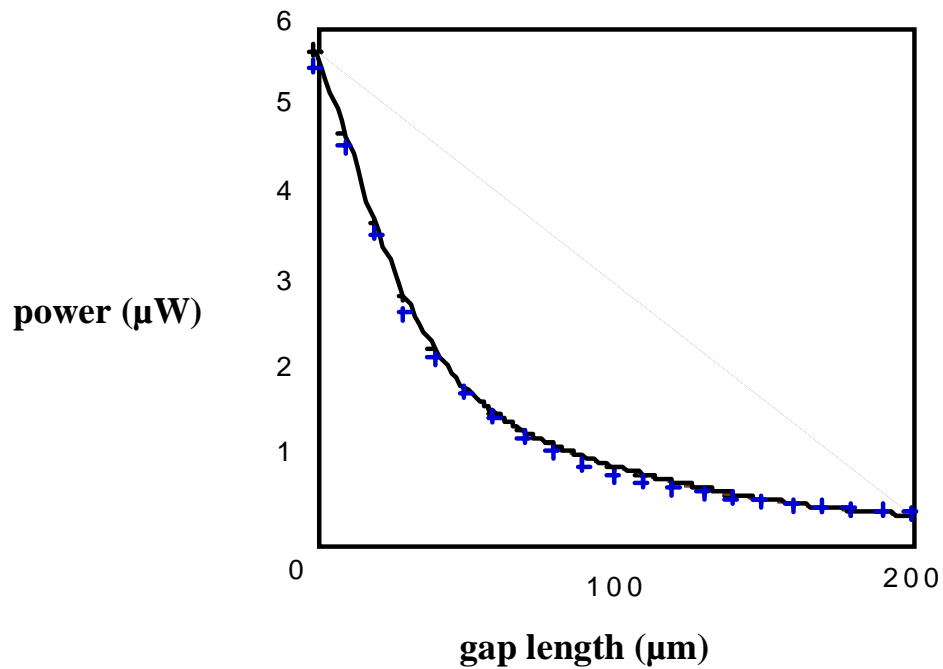


**Figure 1-13. Intensity-based EFPI output transfer function.**

#### **1.2.4.2 White-light Interferometry**

White-light interferometry demodulation allows absolute gap length detection. In white-light interferometry, an EFPI is interrogated with a broadband source, such as a light

emitting diode, and the optical output is fed into an CCD array which converts the optical spectrum into an electrical signal (Figure 1-14). Wavelengths for which the phase difference between the sensing and reference reflections are  $2n\pi$  will interfere constructively and be maximum. The gap length can then determined from [12]

$$L = \frac{\lambda_1 \lambda_2}{2(\lambda_1 - \lambda_2)} \quad (1-5)$$

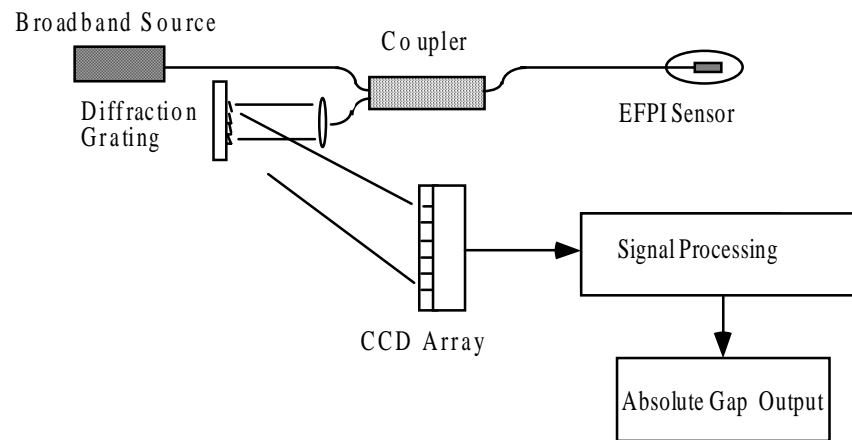


**Figure 1-14. White-light interferometric demodulation setup.**

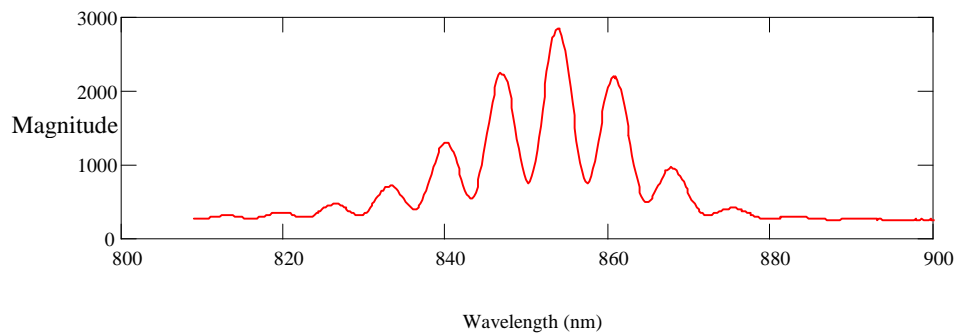


**Figure 1-15. EFPI interferometric output for a gap of 50.45 $\mu$ m.**

This method enables absolute gap length detection. Currently this method is limited to quasi-static gap length changes due to the complexity of the algorithm to find a precise

gap measurement from a broadband spectrum (Figure 1-15). With current algorithms, the resolution is around 5nm with a total dynamic gap range of 20 to 500  $\mu\text{m}$  [12].

### ***1.3 Overview***

Chapter 2 discusses current optical fiber sensor multiplexing topologies and technologies. The difference between serial and spatial multiplexing approaches is discussed. Additionally, the several advantages and disadvantages of different multiplexing approaches, such as TDM, FDM, WDM, etc. are investigated. It also contains an introduction to the idea of optical path length multiplexing and compares OPLM to conventional multiplexing methodologies.

Chapter 3 investigates optical path length multiplexing in depth. It begins with a discussion of the theory and then leads to the results of several tests conducted to find the limits of OPLM. The last part of this chapter presents a demonstration of optical path length multiplexing.

Chapter 4 discusses several demonstrated and possible applications of optical path length multiplexing. Each application is discussed in depth with results from experiments verifying the feasibility of these approaches. This chapter showcases the flexibility of optical path length multiplexing.

Chapter 5 presents the conclusion to the thesis and possible future work. In future work, an in-depth design study of a serially multiplexed thermally compensated pressure sensor system will be implemented. The system will be designed to meet the specified system goals. Additional testing will be performed to determine more limits of optical path length multiplexing.

## **2. Chapter 2 - Optical Fiber Sensor Multiplexing**

In point sensor elements, the measurand can be encoded into the amplitude, phase, polarization, or spectral information of the optical signal. Measurand information can also be translated into the frequency or time domain through light modulation. In a multiplexed optical sensor network, the information must be encoded in loss-insensitive signals. Such losses may be due to microbends in the optical fiber, connectors, splices, environmental effects, and optical link length. The type of optical fiber sensor and demodulation scheme determine the multiplexing topology to use.

### ***2.1 Multiplexing Topologies***

Optical fiber sensor networks have the advantage of combining sensor and transmission medium into a single entity. Multiplexing involves four main functions: powering, detecting, identifying, and evaluating. The basic multiplexing topology chosen depends upon the sensing technology used. Fiber links, splices, connectors, couplers, and other components are used to interconnect the multiplexed sensors. For point reflective sensors (such as the EFPI), there are several different topologies. These topologies can be divided into two main categories; serial multiplexing and spatial multiplexing. [1] Serial multiplexing consists of optical fiber sensors connected end to end on a single strand of fiber (Figure 2-1). Serial multiplexing is another name for discrete distributed multiplexing. Serial multiplexing is useful for measuring not only the magnitude of a measurand, but also its variation along the length of a continuous optical fiber [13].

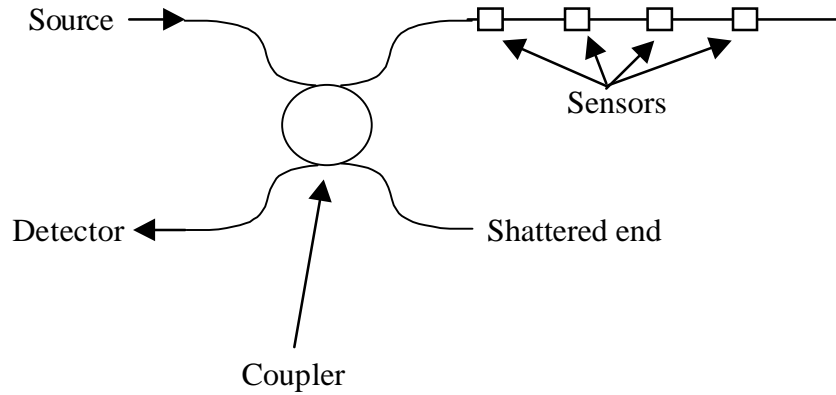


**Figure 2-1. Serial multiplexing topologies.**

Spatial multiplexing consists of an optical fiber strand per optical fiber sensor with one source and one detector. Typical spatial multiplexing topologies are reflective star and reflective tree (Figure 2-2) Spatial multiplexing while more complex and cumbersome than serial multiplexing has its own advantages. Sensors in a spatial multiplexing topology can be more easily replaced in the event of failure, additionally, spatial multiplexing works well in applications for mapping measurands over a two-dimensional surface, in contrast to serial multiplexing, which works well for linear dimensions.

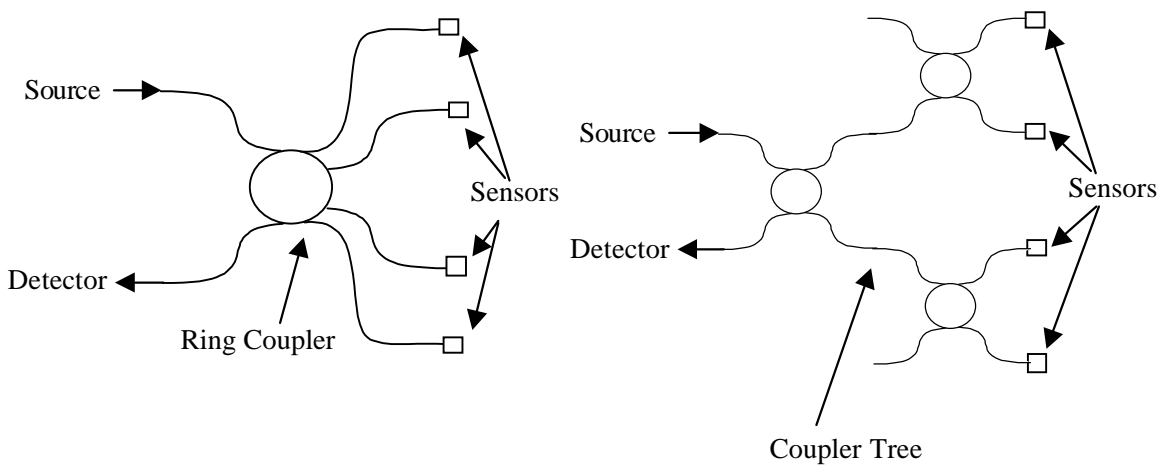


**Figure 2-2. Spatial multiplexing topologies.**

## 2.2 Current Multiplexing Technologies

Table 1 shows a comparison of several different current multiplexing techniques. Current multiplexing technologies include spatial multiplexing, TDM, WDM, and FDM.

Multiplexing method	Advantages	Disadvantages	Comments
Spatial multiplexing	<ul style="list-style-type: none"> <li>• Simple concept.</li> <li>• Excellent power budget.</li> <li>• Single-channel failure may in some cases be tolerated.</li> </ul>	<ul style="list-style-type: none"> <li>• Multiple detectors required.</li> <li>• High cable and connector cost.</li> <li>• Extra weight, volume and less-flexible cabling.</li> <li>• Inter-channel comparison analog signals may be affected by variations in cable or connectors.</li> </ul>	<ul style="list-style-type: none"> <li>• Technically less elegant, but simple to engineer.</li> <li>• May be combined with TDM or WDM in source / monitor terminal unit.</li> </ul>
Time-division multiplexing	<ul style="list-style-type: none"> <li>• Simple electronic decoding.</li> <li>• Single source and detector.</li> <li>• Can have large numbers of channels/fiber.</li> </ul>	<ul style="list-style-type: none"> <li>• Requires fast electronics, unless long optical path differences in sensor.</li> </ul>	<ul style="list-style-type: none"> <li>• Attractive for large number of channels.</li> <li>• May be used with single-fiber, dual-fiber, or multiple-fiber links.</li> <li>• Has been used in both coherent and incoherent systems.</li> </ul>
Wavelength-division multiplexing	<ul style="list-style-type: none"> <li>• Low speed electronics.</li> <li>• Good optical loss budget.</li> </ul>	<ul style="list-style-type: none"> <li>• Multiple sources and detectors necessary.</li> <li>• Difficulties become severe for more than</li> </ul>	<ul style="list-style-type: none"> <li>• May be used with single-fiber, dual-fiber, or multiple-fiber links.</li> </ul>

		10-20 sensor channels/fiber.	
Frequency-division multiplexing of sub-carrier	<ul style="list-style-type: none"> <li>Fairly simple decoding for small number of channels.</li> <li>Single source and detector possible.</li> </ul>	<ul style="list-style-type: none"> <li>Difficulties increase with large number of channels.</li> </ul>	<ul style="list-style-type: none"> <li>May be used with single-fiber, dual-fiber, or multiple-fiber links.</li> </ul>

**Table 1. Comparison of different multiplexing technologies [13]**

### 2.2.1 Spatial Multiplexing

Spatial multiplexing is a simple multiplexing approach in which separate fibers and separate detectors are used to communicate with each separate sensor without cross talk between the signals. A slightly more cost effective approach uses a single source and signal processing electronics and switches between reflective sensing fibers. Spatial multiplexing can be combined with other multiplexing technologies (such as TDM or WDM) to increase the number of sensors interrogated with a single source/signal processing unit.

### 2.2.2 Time Division Multiplexing

Time division multiplexing is a popular multiplexing approach in which different sensors respond in a repeatable sequence. This sequence is achieved by building in optical propagation delays unique to each sensor. When an optical sensor is pulsed, each sensor returns pulses to the detector in sequence. The pulse rate of the source must be slow enough to allow the pulse from the furthest sensor to reach the detector before the next pulse from the nearest sensor reaches the detector [13]. Time division multiplexing suffers from inflexibility in terms of the number of sensor that can be addressed. Because the pulse timing is fixed, bandwidth usage cannot be optimized if the number of sensors

changes. The number of sensors in a TDM scheme is limited not only by power losses, but also by the sampling restrictions. [14]

### 2.2.3 Wavelength Division Multiplexing

Wavelength division multiplexing is a multiplexing system that utilizes optical fiber sensors that respond to unique wavelengths. In wavelength division multiplexing, multiple wavelengths are sent down an optical fiber. Optical filters are then employed to filter out a specific wavelength which is then used to interrogate a specific sensor. The wavelengths returned from the sensors are then recombined in the optical fiber until they are finally separated again at the optical detector and signal processing unit. While optical fiber bandwidth is enormous, wavelength division multiplexing is limited by the optical sources, and the optical filters. In one approach to wavelength division multiplexing, a broadband source, such as an LED, and narrowband optical filters are implemented. Because the bandwidth of the filters is fairly wide relative to a spectral width of the LED source, the maximum number of sensors that can be wavelength division multiplexed is generally less than ten. Another approach to WDM uses multiple narrow line width sources. Narrow line width sources, like narrowband optical filters, are very expensive and only manufactured for limited wavelengths. Growing use of WDM components in telecommunications is lowering their cost and increasing their availability. However, at this time, WDM is not a very popular method for optical fiber sensor multiplexing. [14]

### 2.2.4 Frequency Division Multiplexing

Frequency division multiplexing uses different frequency signals to distinguish between different sensor responses. In a simple FDM system, each sensor may have a separate optical source modulated at different frequencies. The outputs of these sensors can then

be combined into a optical fiber and detector. Signal processing is then used at the detector to filter each sensor signal.

### ***2.3 Optical Path Length Multiplexing***

Optical path length multiplexing is a method in which optical fiber sensors (such as EFPIs) are biased at specific gaps or optical path lengths, and then limited in operation to some specific range around the bias point. These signals can be isolated and tracked through white-light interferometry techniques, provided the individual signals do not interfere with each other. Optical path length multiplexing is very useful for multiplexing a small number of sensors. It is topology independent and can actually work well with numerous different sensor types (EFPI, IFPI, 2-mode, etc.) Optical path length multiplexing also does not require additional sources, detectors, or signal processing electronics over conventional white-light interferometry techniques.

#### ***2.3.1 Use of Optical Path Length Multiplexing with other Multiplexing Techniques***

One advantage of optical path length multiplexing is that it can be easily implemented into other multiplexing technologies to easily double or triple the number of sensors that can be addressed without adding additional hardware to the system. One example of a possible of a hybrid multiplexing scheme, would be to combine OPLM with a basic spatial multiplexing system. Without OPLM, this system (Figure 2-3) consists of eight sensors on a 1x8 switch that switches rapidly between each sensor. With OPLM usually up to three conventional EFPIs could be serially multiplexed on each switched fiber, resulting in a total of 24 sensing channels versus the original eight.

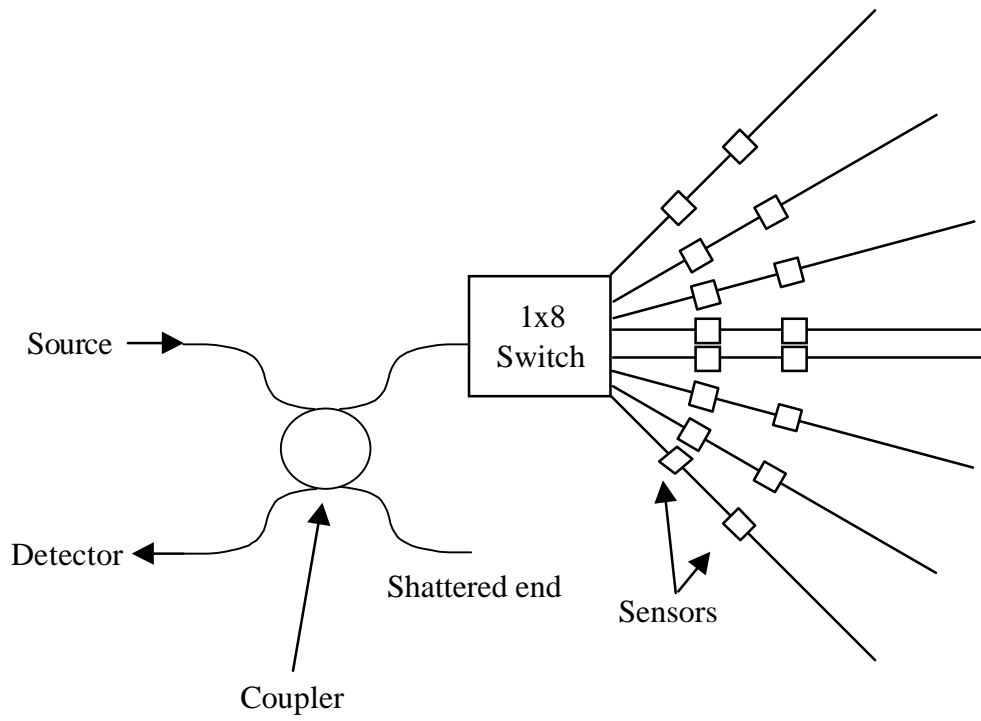


**Figure 2-3. Hybrid spatial multiplexing and optical path length multiplexing system.**

### **3. Chapter 3 - Optical Path Length Multiplexing**

Optical path length multiplexing is a method in which optical fiber sensors (such as EFPIs) are biased at specific gaps or optical path lengths, and then limited in operation to some specific range around the bias point. These signals can be isolated and tracked through white-light interferometry techniques, provided the individual signals do not interfere with each other. Optical path length multiplexing is very useful for multiplexing a small number of sensors. It is topology independent, and can actually work well with numerous different sensor types (EFPI, IFPI, 2-mode, etc.) Optical path length multiplexing does not require additional sources, detectors, or signal processing electronics over conventional white-light interferometry techniques.

#### ***3.1 Theory***

In one approach to white-light interferometry, a spectrum such as Figure 3-2, converted into an electrical signal by a spectrometer, is fed into a computer. Signal processing is performed in the computer to find the absolute gap of the EFPI from the spectrum. The first step in finding the absolute gap from this spectrum is to look at the power spectral density of the spectrum. A sample spectrum of two multiplexed EFPIs is shown as Figure 3-1. The output of the power spectral density is shown in Figure 3-2.

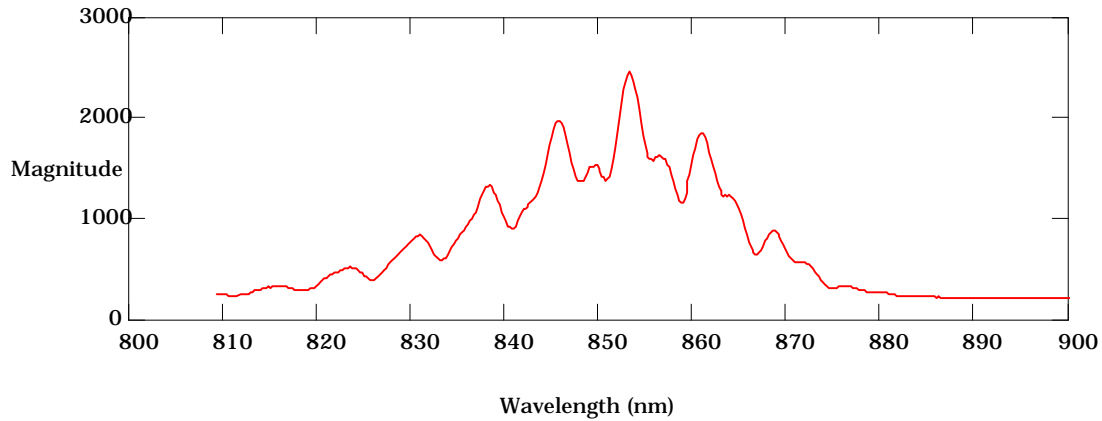


**Figure 3-1. EFPI interferometric output for two multiplexed sensors.**

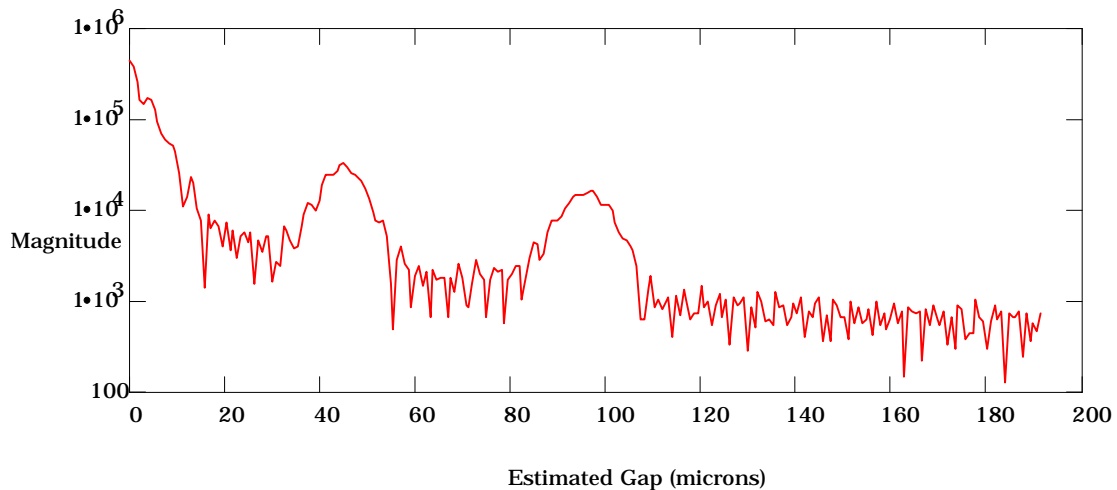


**Figure 3-2. Power spectral density for two multiplexed sensors.**

The next step in a conventional white-light demodulation algorithm finds the highest intensity sensor peak over the entire PSD. In the final stage of demodulation, a peak search algorithm is performed to find the exact absolute gap from the sensor peak. In optical path length multiplexing, the power spectral density contains multiple sensor peaks. The peak search algorithm is then performed on each sensor peak. Therefore by defining operating ranges for each sensor, multiple sensors can be interrogated and tracked with no additional hardware than that of a typical white-light interferometric demodulation system. These sensors can be either serially multiplexed (all in the same

fiber) or spatially multiplexed (using a star coupler.) For example, suppose two sensors are gap division multiplexed; the first sensor might have a gap range of 50 $\mu\text{m}$  to 100 $\mu\text{m}$  and the second sensor, a gap range of 150 $\mu\text{m}$  to 200  $\mu\text{m}$ .

### 3.2 Tests to find minimal buffer zone

The first question to address with the concept of optical path length multiplexing is to find the minimal buffer needed between sensor gap ranges so that the multiplexed signals do not interfere. To resolve this question, an EFPI sensor with a 50  $\mu\text{m}$  gap and a variable gap low-profile EFPI sensor were used at a source wavelength of 830 nm. These sensors were connected via a coupler to the source/detector system (Figure 3-3). Figure 3-4 shows a close-up of a low-profile variable gap EFPI. It consists of an optical fiber polished at 45 degrees positioned over a gold coated glass slide. Using a vertical positioner to move the gold coated glass slide, the gap length was adjusted. The variable gap low-profile EFPI started with a gap of 50  $\mu\text{m}$ , which was increased in 1  $\mu\text{m}$  intervals up to 80  $\mu\text{m}$ .

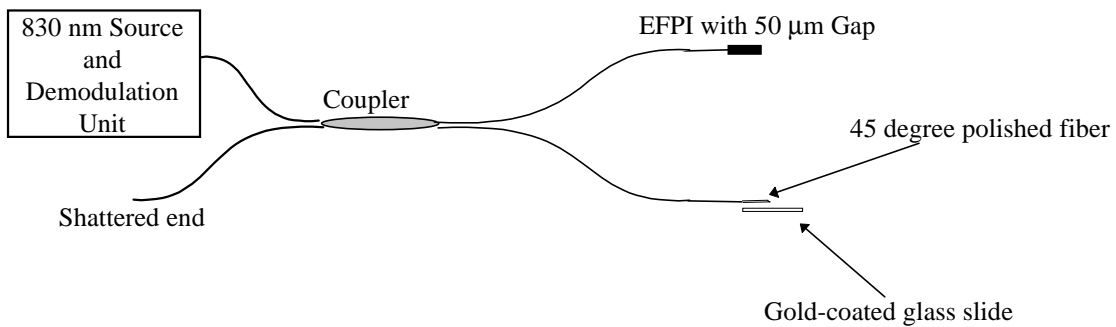


**Figure 3-3. Buffer zone testing setup.**

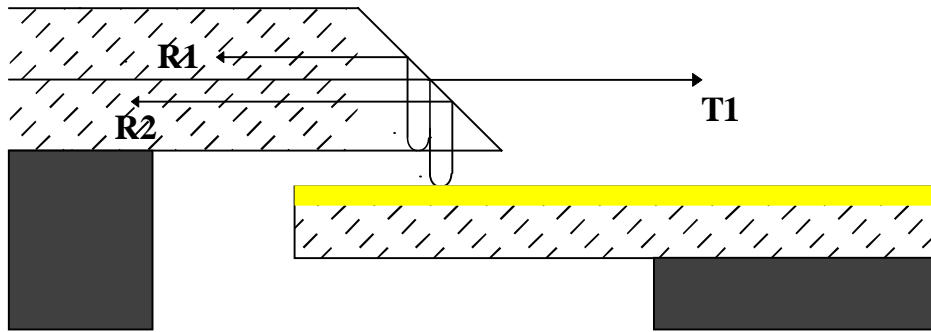


**Figure 3-4. Variable gap EFPI setup.**

At the start of the test, the variable gap low-profile EFPI was set to a gap of 50  $\mu\text{m}$ . Figure 3-5 shows the returned spectrum and the demodulated signal from this setting. The wave spectrum shows only one sensor. The demodulated signal shows one peak. A gap around 50  $\mu\text{m}$  can be seen, but because of the width of the peak due to the additional sensor at 50  $\mu\text{m}$ , an exact gap measurement cannot be accurately determined.

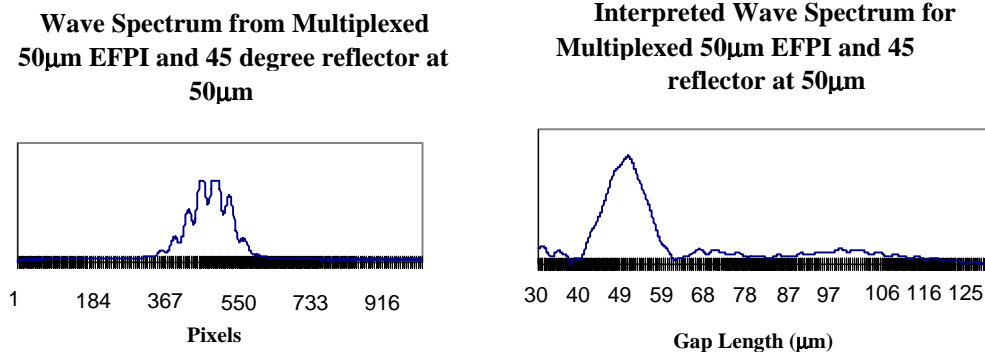


**Figure 3-5. a) Returned wave spectrum from two multiplexed EFPIs. b) Power spectral density showing two EFPI sensor peaks at 50  $\mu\text{m}$ .**

At another interval the variable gap low-profile EFPI was set to a gap of 65  $\mu\text{m}$ . Figure 3-6 shows the returned spectrum and the demodulated signal from this setting. The wave spectrum barely shows a multiplexed sensor. The demodulated signal shows one major

peak and the beginnings of a second peak. However, the presence of the second sensor so close to the first corrupts the demodulation as each of the peaks are pulled closer to each other. Thus, there are peaks at 51  $\mu\text{m}$  and 64  $\mu\text{m}$ , instead of a peak at 50  $\mu\text{m}$  and 65  $\mu\text{m}$ .

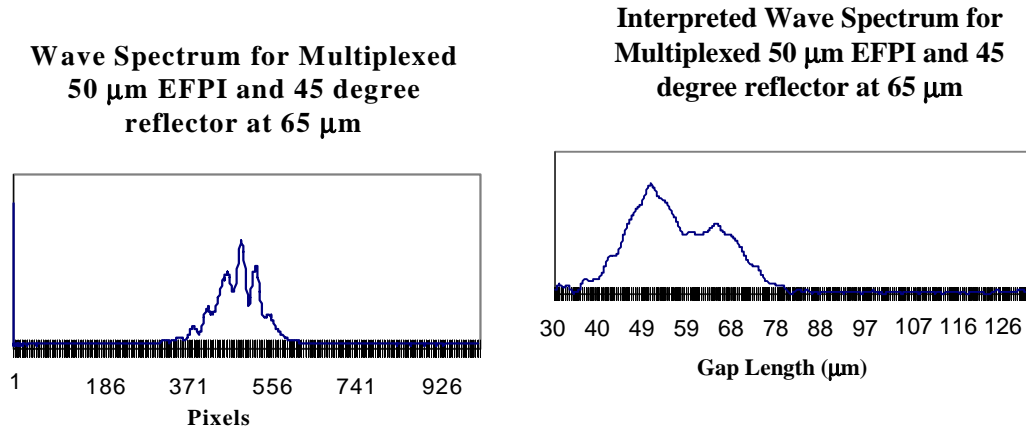


**Figure 3-6 a) Returned wave spectrum from two multiplexed EFPIs. b) Power spectral density showing one EFPI sensor peak at 50  $\mu\text{m}$  and another smaller peak around 65  $\mu\text{m}$ .**

At the last interval, the variable gap low-profile EFPI sensor was set to a gap of 80  $\mu\text{m}$ . Figure 3-7. shows the returned spectrum and the demodulated signal from this setting. The wave spectrum clearly shows a multiplexed sensor. The demodulated signal shows two distinct peaks. The sensor gap buffer is large enough such that the signals do not corrupt each other. While a second peak can be seen as low as 15  $\mu\text{m}$  apart, for a multiplexed system, the minimal gap operating range buffer should be 30  $\mu\text{m}$ .

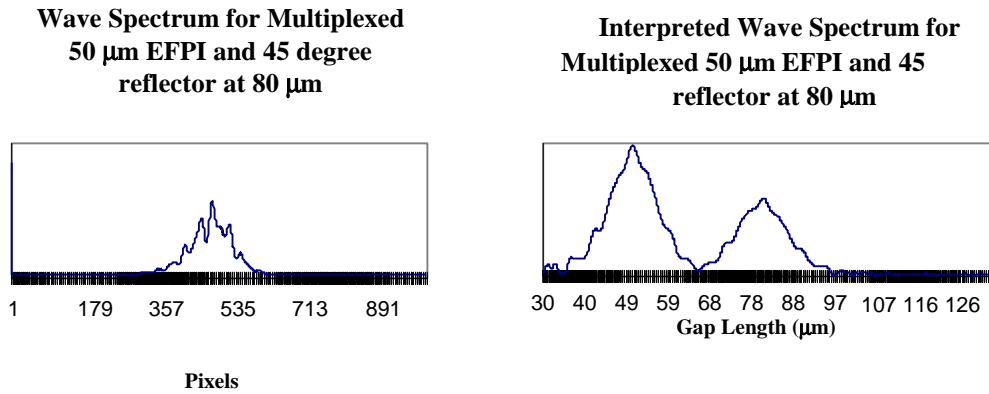


**Figure 3-7. a) Returned wave spectrum from two multiplexed EFPIs. b) Demodulated wave spectrum showing one EFPI sensor peak at 50 μm and another smaller peak around 80 μm.**

### 3.3 Tests for double gap

Another concern for optical path length multiplexing is the phenomenon of double gap signals. The higher the reflective coefficient of the reflecting fiber in an EFPI, the greater the power of the second reflection. If this second reflection is strong enough, it can reflect off of the source fiber and then reflect of the reflector a second time to generate R3 (Figure 3-8). The interferometric signal between R1 and R3 produces an effective double gap signal.

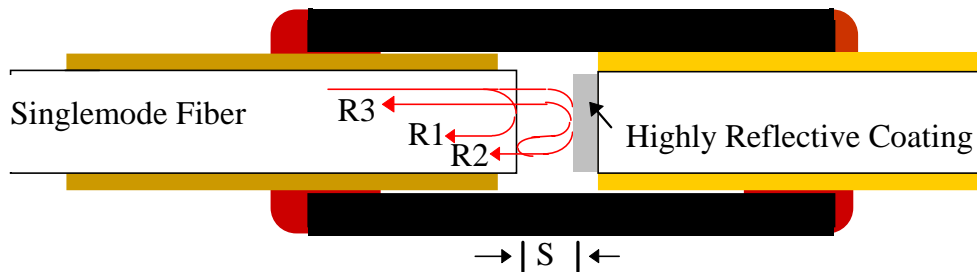


**Figure 3-8. EFPI Sensor with highly reflective reflector to generate double gap effect.**

One possible limitation of optical path length multiplexing is this double gap effect. Typical EFPIs are constructed with either an optical fiber or metallic coated fiber. The reflectivity of fused silica optical fiber is about 4% while the reflectivity of a metallic coating (gold, chromium, etc) at 830 nm is around 97%. Tests were conducted to see if two EFPI sensors with fused silica reflectors could be multiplexed if their gaps were integral multiples. For this test two EFPI sensors were multiplexed with gaps of 50  $\mu\text{m}$  and 100  $\mu\text{m}$ . These sensors were connected via a coupler to the source/detector system (Figure 3-9). The wave spectrum and power spectral density containing the information from both EFPI sensors can be seen in Figure 3-10. After a power spectral density calculation on the wave spectrum, the two peaks representing the two multiplexed sensors are distinguishable. Thus, it was successfully shown that multiplexed EFPIs with fused silica reflectors can operate at gaps that are integral multiples of each other because the reflection from fused silica reflectors is not strong enough to generate a double gap.

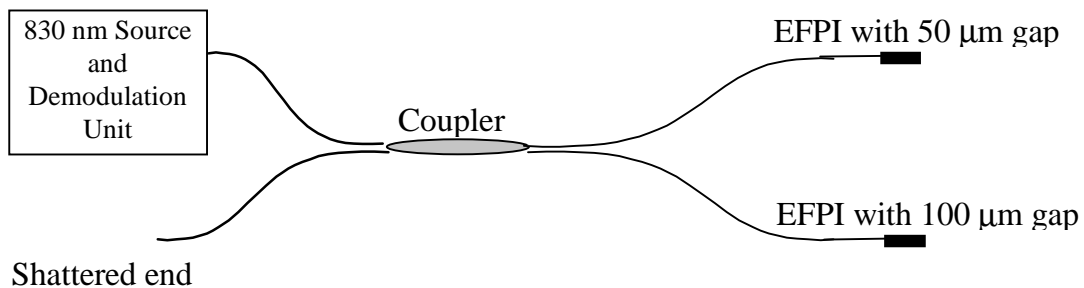


**Figure 3-9. Test for double gap.**

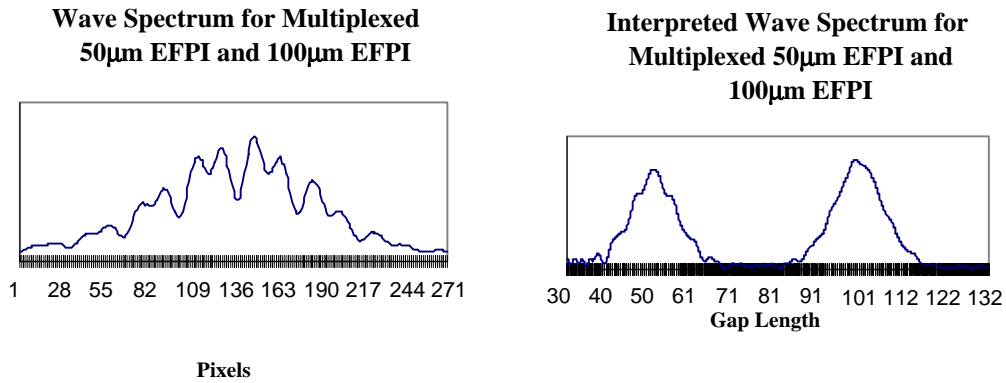
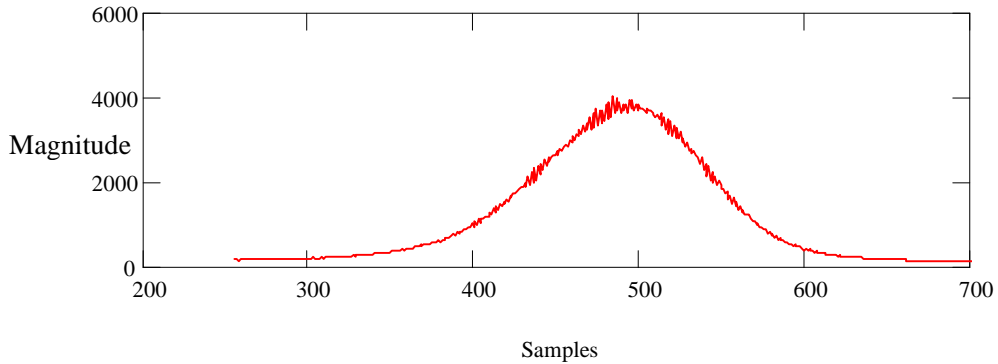


**Figure 3-10. a) Returned wave spectrum from two multiplexed EFPIs both with 50 µm gaps. b) Demodulated wave spectrum showing one EFPI sensor peak around 50µm.**

### ***3.4 Theoretical limits of operation***

When designing a optical path length multiplexed system, there are several factors to take into consideration. From the results of section 3.2, OPLM sensors must be at least 30 µm apart to ranges maintain gap measurement integrity. Another limitation of OPLM is that EFPI sensors with metallic reflectors can generate double, triple, and on occasion, even quintuple gap signals. In the design of an OPLM system, EFPI operating ranges must be established with these considerations. Conventional white-light interferometry demodulation techniques are used to monitor gaps between 30 and 300 µm. However, the variable gap EFPI with the gold reflector was still discernible at a gap of 918 µm (Figure 3-11). With the conventional range of 270 µm, and a minimum 30 µm buffer between each signal, the maximum number of sensors that could be multiplexed is ten. With a larger operating range, and only a 20 µm buffer between each operating range, the number of sensors addressed with optical path length multiplexing can be increased. The largest number of independent OPLM sensors tested during this research was three,

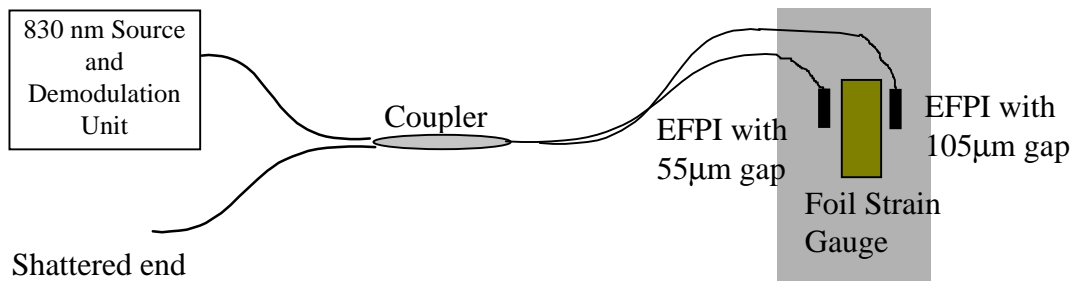
however the largest number of traceable sensor peaks from a power spectral density seen was ten.



**Figure 3-11. Spectrum of variable gap EFPI at 918  $\mu\text{m}$ .**

### ***3.5 Verification of Optical Path Length Multiplexing***

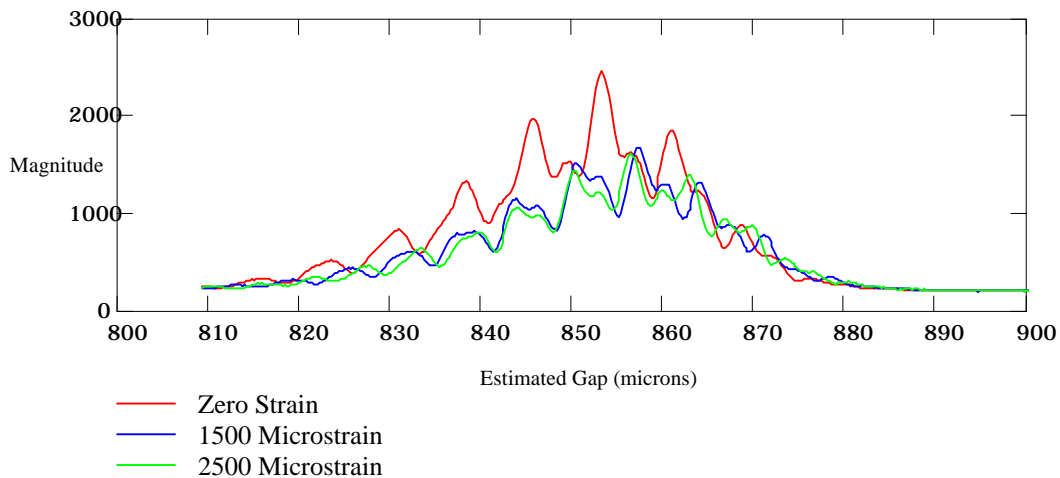
To verify that sensors could be multiplexed via OPLM and maintain their measurement integrity, two EFPI strain sensors were attached to 8-3/4" x 1/2" aluminum beam collocated with a conventional foil strain gage (Figure 3-12). The gauge length of each optical sensor was around 5 mm.



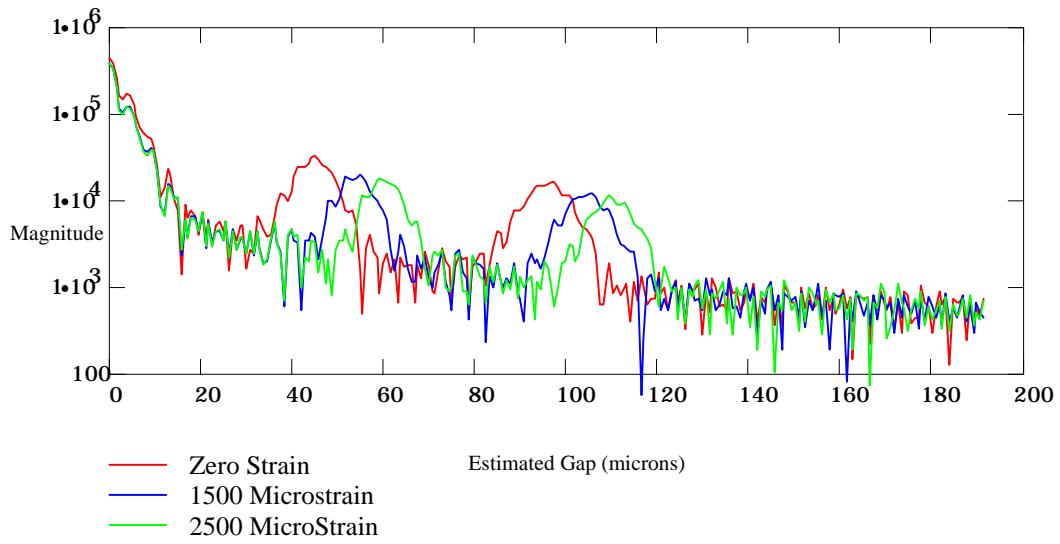
**Figure 3-12. Optical path length multiplexing verification test setup.**

Figure 3-13 shows the returned spectrum from the two multiplexed strain sensors for three different strain values: 0, 1500, 2500  $\mu\epsilon$ . The spectrums for the different strains look fairly comparable except for a drop in the spectrum intensity. The power spectral density over the three strains is shown in Figure 3-14. The sensor peaks can be clearly seen to shift with increasing strain. The sensor gaps are far enough apart such that sensor peaks do not overlap.

Figure 3-15 shows a plot of the EFPI strain gauges versus the foil over time. The multiplexed EFPI sensors match the foil gauge reasonably well. This test verifies that optical path length multiplexing does not effect the accuracy or performance of any multiplexed sensor, provided they are at least 30  $\mu\text{m}$  apart.



**Figure 3-13. Spectrums of two multiplexed EFPIs at three different strains.**



**Figure 3-14. Power spectral densities of two multiplexed EFPIs at three different strains.**

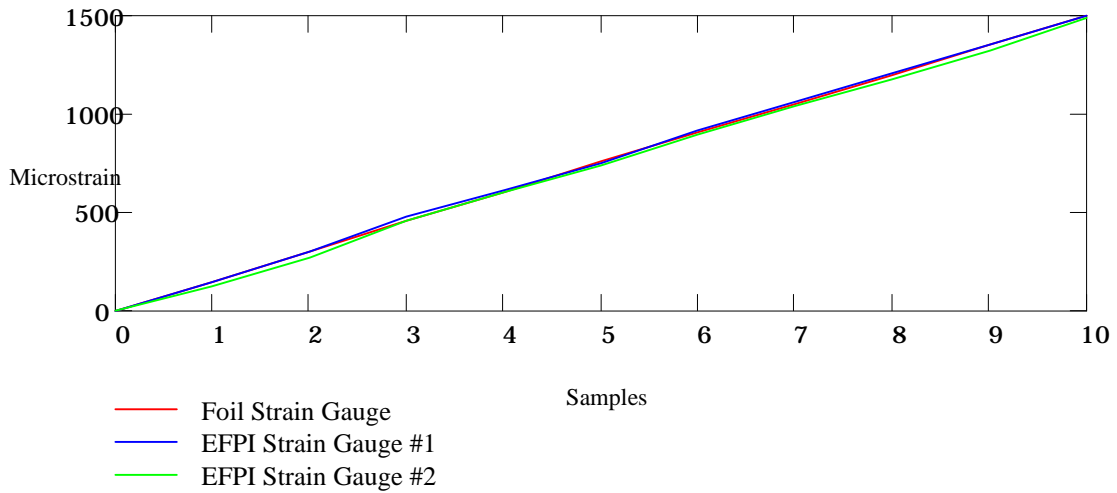


**Figure 3-15. Two multiplexed EFPIs and a foil strain gauge**

## **4. Chapter 4 - Applications of Optical Path Length Multiplexing**

Optical path length multiplexing has numerous applications. It can be used to spatially multiplex any number of EFPI-type pressure, acceleration, force, strain, magnetic field, etc. sensors via coupler trees or rings. Additionally it can be used to serially multiplex EFPI strain sensors or low-profile EFPI-type pressure, acceleration, and force sensors. A third application of OPLM is the ability in diaphragm-based sensors, to track the optical "thickness" of the diaphragm over temperature and use it for temperature measurement and thermal compensation.

### ***4.1 Multiplexed Extrinsic Fabry-Perot Interferometers***

One application of optical path length multiplexing involves serially multiplexing EFPI strain sensors. In serially multiplexed EFPIs, the reflector fiber is not shattered at the end, but leads to the next EFPI sensor. One use of serially multiplexed EFPI strain sensors is to monitor strain or vibration modes along a beam or joint.

As a demonstration of this application, three EFPI strain sensors were serially multiplexed (Figure 4-1). These EFPI sensors, unlike conventional EFPI sensors used 130  $\mu\text{m}$  hollow core fiber to align the fiber endfaces. In a conventional EFPI the reflecting fiber is used as only a mirror and because the refractive index of the core is approximately the refractive index of the cladding, the reflectance across the fiber reflector is relatively constant. Smaller hollow core was needed to provide better optical alignment between the source and reflecting fiber. During construction of this sensor chain, it was found that the third sensor needed a gold or other high reflectance coating to provide a strong enough signal from the sensor for tracking.

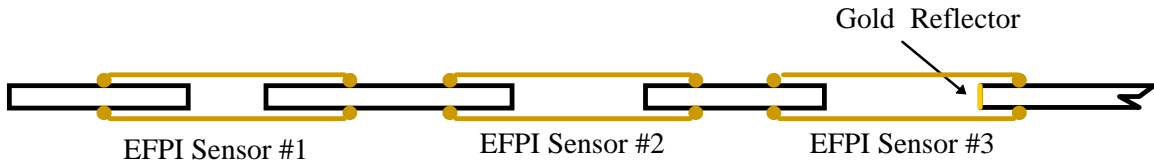


**Figure 4-1. Three serially multiplexed EFPIs.**

Figure 4-2 shows the spectrum returned from the sensors. Due to the shape of the fringe pattern of this spectrum, it can be seen that there are multiplexed sensor signals within it. Figure 4-3 shows the power spectral density of the spectrum. This plot clearly shows the three sensor peaks corresponding to the three serially multiplexed EFPI sensors.

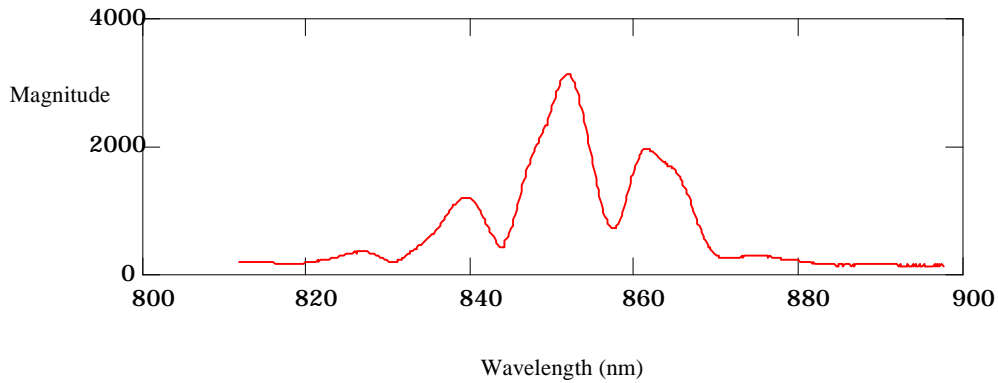


**Figure 4-2. Multiplexed EFPI spectrum.**

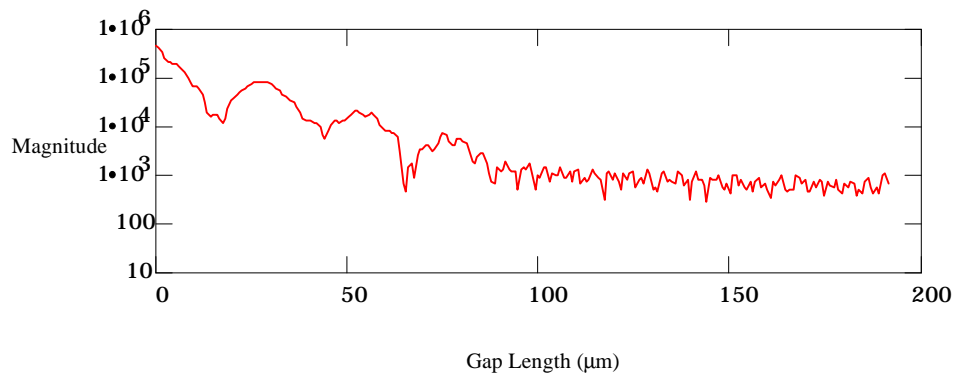


**Figure 4-3. Multiplexed EFPI power spectrum.**

The three multiplexed EFPIs were mounted to a beam which was pulled and then released. Figure 4-3 shows the absolute gap movement of each of the sensor peaks. At one point during the test, the signal from the first EFPI sensor was too close to the noise floor and the signal was lost and then regained later. It can clearly be seen that each of the sensors produced reasonable and repeatable results.

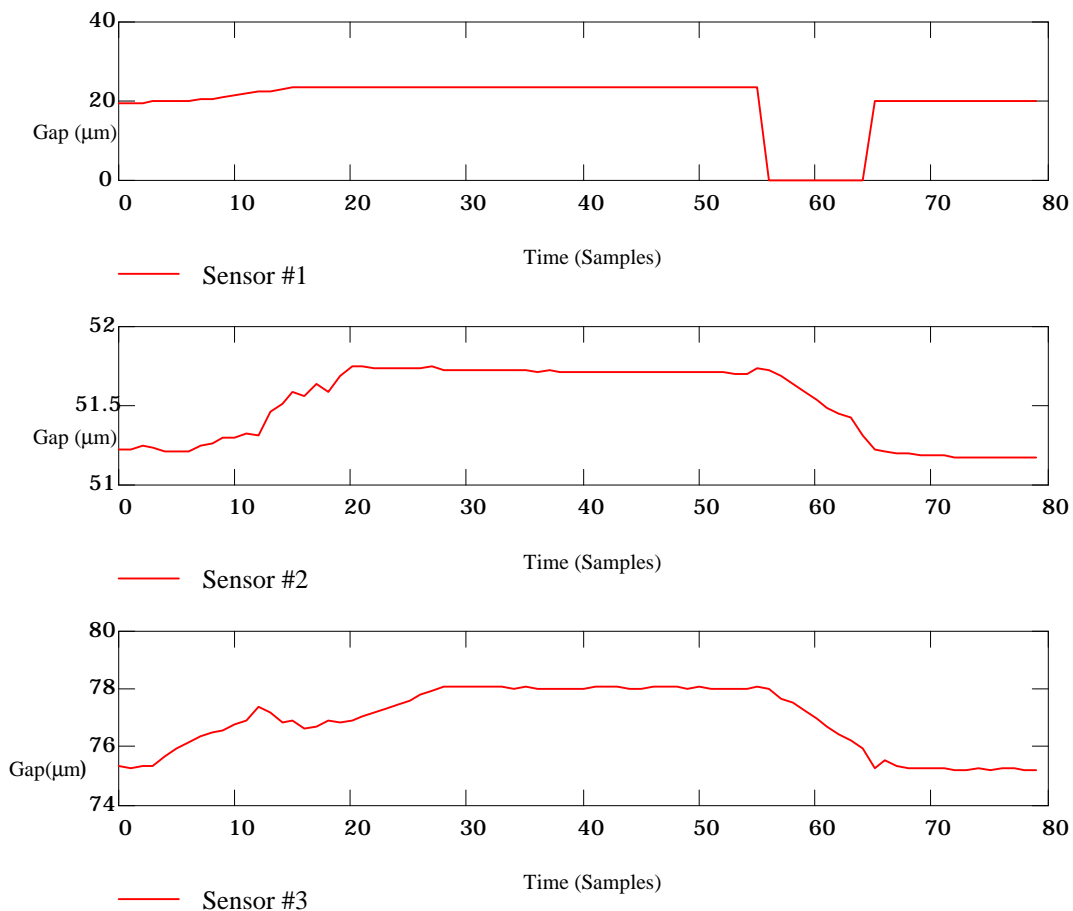


**Figure 4-4. Multiplexed EFPI operation.**

With an 830 SLED source and conventional EFPI strain gauges, three is the maximum that can be serially multiplexed. By using dielectric coatings to change the fiber-air interface, more EFPIs could possibly be serially multiplexed.

## 4.2 Multiplexed Two-mode Sensors

In the course of this testing, it was found that a two-mode sensor [15] could be made by using 1300 nm optical fiber with an 830 nm SLED source. Because the core of the 1300 nm fiber is larger than 830 nm, a second mode is launched into the optical fiber. At connectors, splice tubes, and EFPI air gaps it is believed that mode mixing occurs which produces an interferometric signal between the two modes. This interferometric mode mixing can be resolved as a "gap". In one test, a cleaved section of 1300 nm fiber was connected to an 830 nm source via a splice tube. As the length of the 1300 nm fiber was shortened, the corresponding "gap" measurement changed as well at a rate of around 3-4  $\mu\text{m}$  of gap change per 1 cm of optical fiber.

Two-mode sensors of this type were used to measure distributed force (Figure 4-5) and distributed temperature (Figure 4-6).

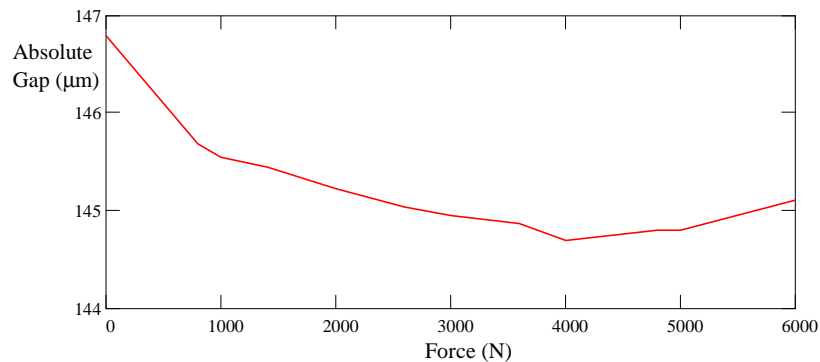


**Figure 4-5. Two-mode force sensor results.**

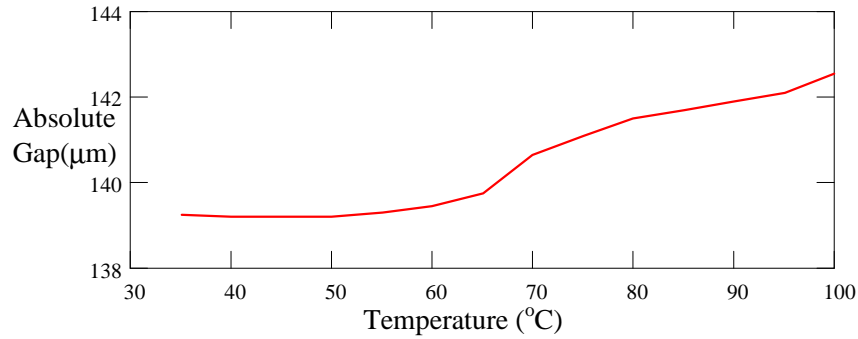


**Figure 4-6. Two-mode temperature sensor.**

These interferometric two-mode sensors can be optical path length multiplexed with themselves or conventional EFPI sensors. Through OPLM, distributed two-mode sensors could be serially multiplexed similar to the EFPIs in section 4.1. Another powerful application of OPLM would be the combination of serially multiplexed EFPIs and two-mode sensors. A sensor system such as this could theoretically be used to measure a distributed strain with point strain measurements at the each end of the distributed section.

Figure 4-7 shows the spectrum returned from a two-mode sensor serially multiplexed with a conventional EFPI sensor. Figure 4-8 is the power spectral density of the spectrum and the sensor peaks for both the two-mode and the EFPI sensor can be seen.

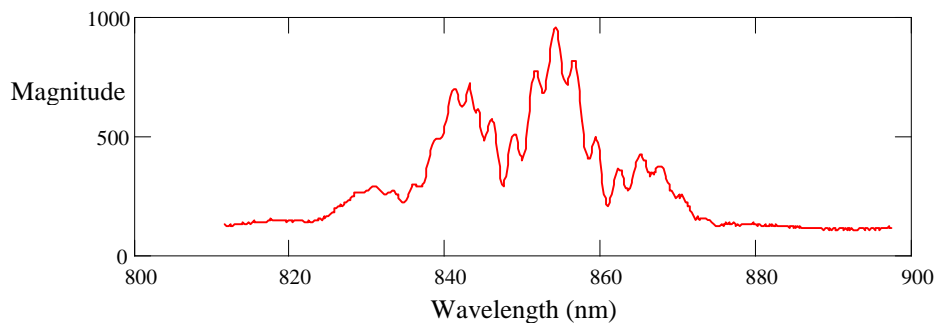


**Figure 4-7. Spectrum of a multiplexed EFPI and a two-mode sensor.**

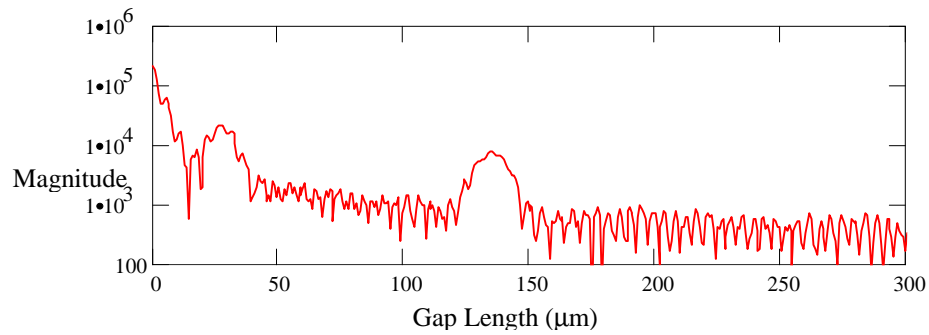


**Figure 4-8. Power spectral density of multiplexed EFPI and two-mode sensor.**

To verify that the two-mode sensor and EFPI were independent of each other, strain was applied to the EFPI sensor (Figure 4-9) alone. From this plot, it is clear that the EFPI strain sensor operated independently of the two-mode sensor. Thus proving a hybrid system of these two sensor types may be possible through optical path length multiplexing.

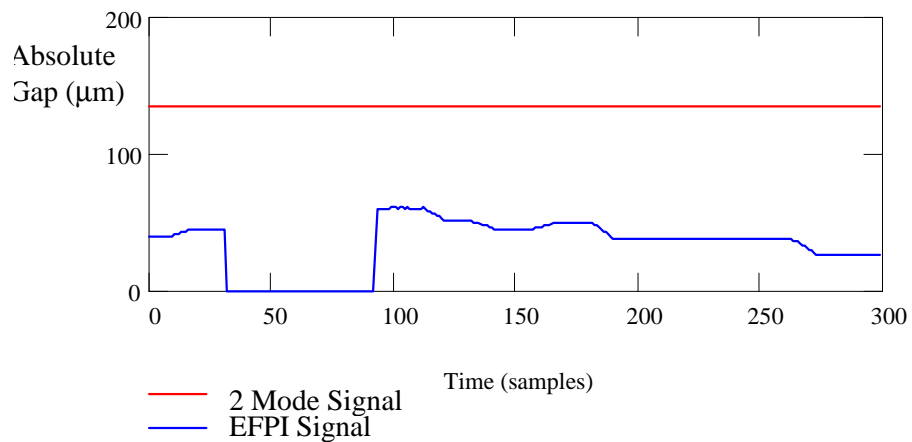


**Figure 4-9. EFPI and two-mode sensors.**

### 4.3 Hybrid Temperature and Pressure Sensor

Another exciting application of optical path length multiplexing is to thermally compensate diaphragm-based EFPI sensors by utilizing a refractive index change of the diaphragm to detect temperature. In an EFPI-type fiber-optic pressure transducer, three interferometric signals are returned to the fiber from the diaphragm (Figure 4-10). The first signal is caused by the interference of a reflection from the end of the fiber (R1) and a reflection from the near side of the diaphragm (R2). The second signal is caused by the interference of a reflection from the near side of the diaphragm (R2) with the light that travels through the diaphragm and reflects off the far side of the diaphragm (R3). The third signal is caused by the interference of a reflection from the end of the fiber (R1) and a reflection from the far side of the diaphragm (R3).

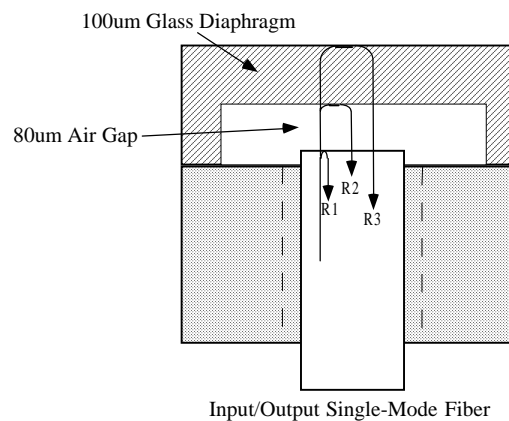


**Figure 4-10. Hybrid temperature/pressure sensor design.**

A pressure transducer was constructed with an air gap of around 80  $\mu\text{m}$  and a diaphragm thickness of 100  $\mu\text{m}$ . This transducer was connected to a source/detector box interfaced with a laptop computer. The returned wave spectrum and demodulated spectrum can be seen in Figure 4-11.

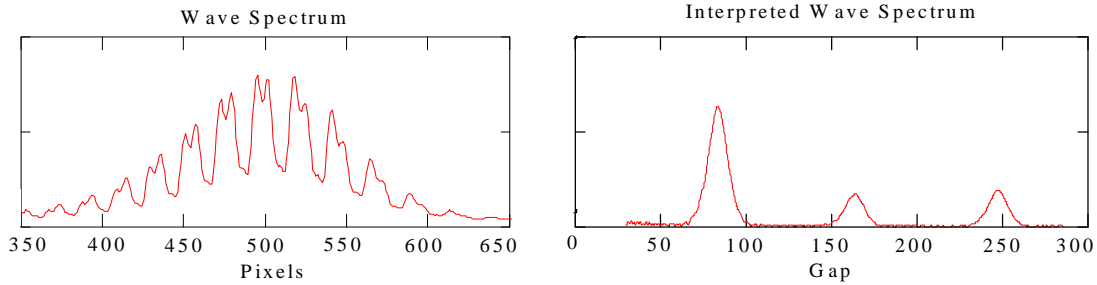


**Figure 4-11. a) Returned wave spectrum from the pressure transducer. b) Demodulated spectrum showing the three signals detected: the air gap, the glass thickness, and the combination of the two.**

The tip of each of the sensor peaks is the measured gap length of each sensor. The first peak, at around 80  $\mu\text{m}$ , tracks the air gap between the fiber and the diaphragm. The second peak, at around 160  $\mu\text{m}$ , tracks the thickness of the glass diaphragm. The demodulation system is designed to measure air gaps. Because the second peak is measuring the thickness of glass and not air, one must divide by 1.5 (the approximate index of refraction of glass) to get the actual thickness of the glass diaphragm. After this adjustment, the thickness of the diaphragm is measured around 100  $\mu\text{m}$ , which matches the actual thickness. The third peak at around 240  $\mu\text{m}$  tracks the air gap plus the thickness of the glass. To verify this interpretation of the three signals theoretically, the measured value of the third peak was compared to the summation of the first two peaks. The third peak measurement was within 0.05% of the summation of the first two peaks.

In measuring the glass thickness over a temperature range, the value will vary due to the refractive index change of the glass; the actual change in the thickness of the glass will be negligible. By dividing the measured glass thickness by the actual glass thickness, the change in index of refraction with changing temperature can be tracked. By measuring the change in index of refraction of glass to measure temperature, the pressure transducers can be thermally compensated. This method of thermal compensation has several advantages. The main advantage is that it does not require any additional sensors

to measure temperature. A secondary advantage is that it measures temperature at the same location it measures pressure.

Figure 4-12 is a plot of the optical thickness of the glass diaphragm over temperature. It shows a change in the optical thickness of the diaphragm of about 5 nm/°C.

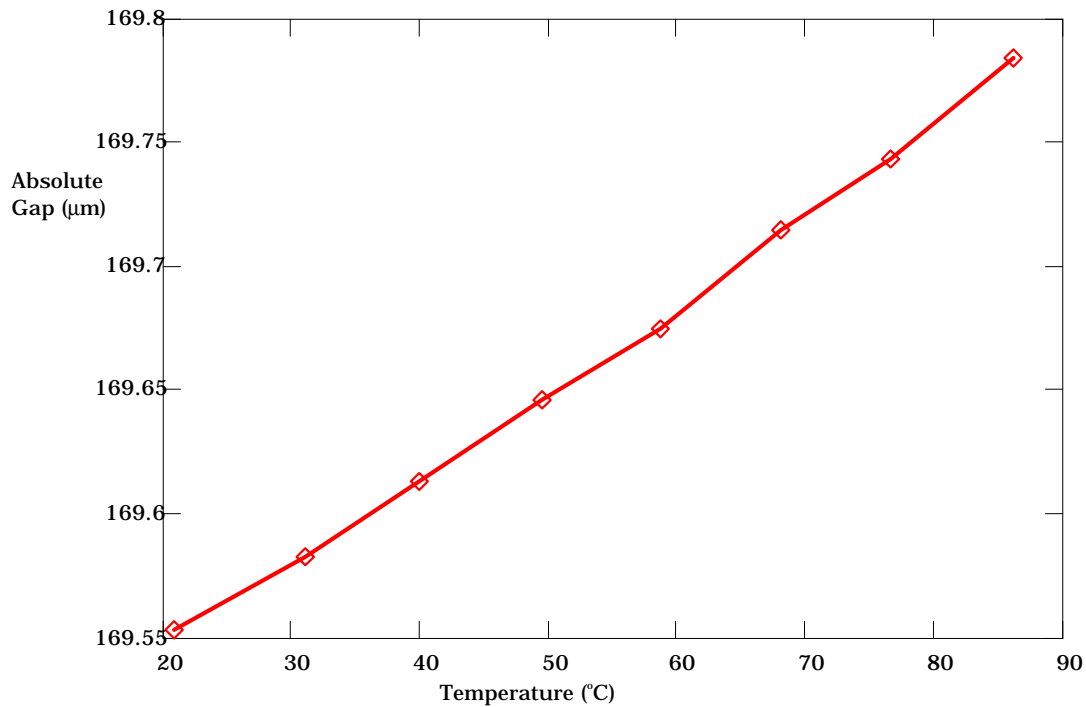


**Figure 4-12. Temperature detection with sensor diaphragm.**

#### ***4.4 Low-profile Extrinsic Fabry-Perot Interferometers***

A final application of optical path length multiplexing is the use of serial or spatially multiplexed low-profile sensors. Using partially reflective angled dielectric coatings, a serially multiplexed system of low-profile sensors can be designed. The dielectric coatings reflect a certain percentage of light as well as transmit a certain percentage of light. Because this is a reflective system, each dielectric coating has a cumulative effect

on the power loss in the system. For a three low-profile sensor system, calculations were performed to find the dielectric coatings that would return equal power to the source. After extensive calculations, the splitting ratio of the dielectric coatings was found to be 30/70, 50/50, and 98/2.

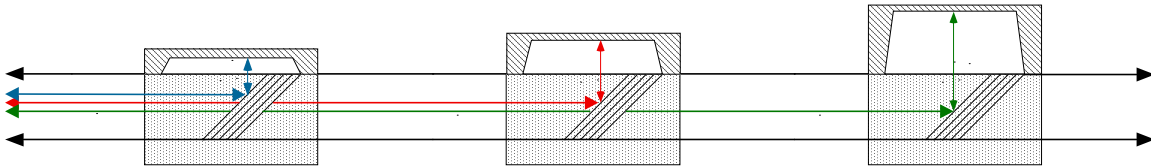


**Figure 4-13. Low-profile multiplexing design.**

Multiplexed low-profile sensors have several applications in industry. One example is a system that would use low-profile pressure sensors to map pressure across a surface.

## **5. Chapter 5 - Conclusions and Future Work**

### ***5.1 Conclusion***

Optical fiber sensor multiplexing reduces cost per sensor by designing a system that minimizes the expensive system components (sources, spectrometers, etc.) needed for a set number of sensors. The market for multiplexed optical sensors is growing as fiber-optic sensors are finding application in automated factories, mines, offshore platforms, air, sea, land, and space vehicles, energy distribution systems, medical patient surveillance systems, etc. Optical path length multiplexing is a modification to traditional white-light interferometry techniques to multiplex extrinsic Fabry-Perot interferometers and optical path length two-mode sensors. Additionally, OPLM techniques can be used to design an optical fiber sensor to detect pressure/force/acceleration and temperature simultaneously at a single point. While power losses and operating range restrictions limit the large-scale applicability of OPLM, it provides a way to easily double or quadruple the number of sensors by modifying the demodulation algorithm. The exciting aspect of OPLM is that no additional hardware is needed to multiplex a few sensors. In this way OPLM works with conventional technology and algorithms to drastically increase their efficiency. [1]

### ***5.2 Future Work***

One of the future goals of this project is to further develop optical path length multiplexing. One question that remains to be answered is how much power is actually needed to demodulate an EFPI sensor? By finding the answer to this question, the operating parameters for OPLM can be established.

Another goal of this project to be realized is the construction of a system of three thermally compensated low-profile pressure sensors (Figure 5-1). The pressure sensors will have a 15  $\mu\text{m}$  thick silicon diaphragms. Because the refractive index of silicon is approximately 2.4, the optical thickness of the diaphragm will be around 36  $\mu\text{m}$ . The pressure sensors will be biased at gaps of 75 , 150, and 225  $\mu\text{m}$ . These sensors will be thermally compensated by tracking temperature with change in the optical thickness of the diaphragm. Thus the complete OPLM system will simultaneously track six signals (75, 75+36, 150, 150+36, 225, and 225+36) to determine pressure and temperature at three distinct points (Figure 5-2).

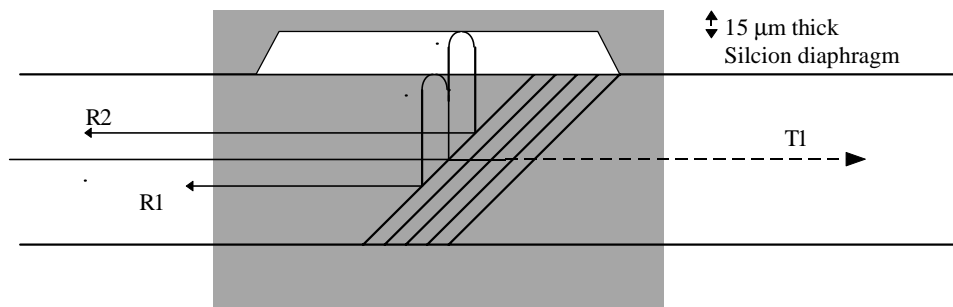


**Figure 5-1. Thermally compensated pressure sensor system design.**

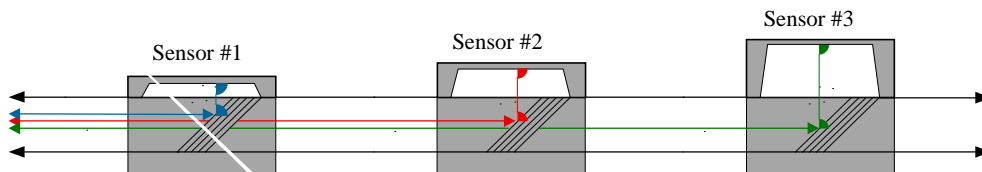


**Figure 5-2. Multiplexed pressure sensor system design.**

## References

1. B. Culshaw, Optical Fiber Sensors: Systems and Applications, Artech House, Norwood, MA, 1989.
2. E. Udd, Fiber Optic Sensors: An Introduction for Engineers and Scientists, John Wiley and Sons, NY, 1991.
3. D.A.Jackson, Selected Multiplexing Schemes For Fibre Optic Interferometric Sensors, Distributed and Multiplexed Fiber Optic Sensors III, SPIE, Boston, MA, 1993.
4. Scott Meller, "Extrinsic Fabry-Perot Interferometer System Using Wavelength Modulated Source," *Master's Thesis*, Virginia Polytechnic Institute and State University, Blacksburg, VA, 1996.
5. J.L. Santos, A.P. Leite, and D.A. Jackson, "Optical fiber sensing with a low-finesse Fabry-Perot cavity," *Applied Optics*, Vol. 31, No. 34, pp.7361-7366, December 1992.
6. Kent A. Murphy, Michael F. Gunther, Ashish M. Vengsarkar, and Richard O. Claus, "Quadrature phase-shifted, extrinsic Fabry-Perot optical fiber sensors," *Optics Letters*, Vol.16, No. 4, pp.273-275, February 1991.
7. Kent Murphy, "Novel phase-modulated optical fiber sensors," *Doctoral Dissertation*, Virginia Polytechnic Institute and State University, Blacksburg, VA, 1992.
8. K.A. Murphy, "Multiplexed extrinsic Fabry-Perot interferometers and applications," *Distributed and Multiplexed Fiber Optic Sensors V*, SPIE, Munich, FRG, 1995.

9. Di Giovanni, Mario, Flat and Corrugated Diaphragm Design Handbook, Marcel Dekker, Inc., New York, 1982.
10. Kristl B. Hathaway and Arthur E. Clark, "Magnetostrictive Materials," *MRS Bulletin*, pp. 34-41, April 1993.
11. Jong-Dug Shin, "Dielectric Mirror Embedded Optical Fiber Couplers," *IEEE Journal of Light Wave Technology*, Vol.12, No. 1, pp.68-73, January 1994.
12. Vikram Bhatia, "Signal Processing Techniques for Optical Fiber Sensors Using White Light Interferometry," *Master's Thesis*, Virginia Polytechnic Institute and State University, Blacksburg, VA, 1993.
13. J.P. Dakin, Distributed Fibre Optic Sensing Handbook, IFS Publications, UK, 1990.
14. Mohit Bhatnagar, "Multiplexing of Interferometric Fiber Optic Sensors for Smart Structure Applications using Spread Spectrum Techniques," *Master's Thesis*, Virginia Polytechnic Institute and State University, Blacksburg, VA, 1994.
15. Shang-Yuan Huang, "Perturbation Effects on Mode Propagation in Highly Elliptical Core Two-Mode Fibers," *IEEE Journal of Light Wave Technology*, Vol.8, No. 1, pp.23-33, January 1990.

## **Vita**

Thomas Wavering was born in Fairfax, Virginia on January 20, 1974. He graduated with a Bachelor of Science degree in Electrical Engineering with a minor in Creative Writing - Poetry from Virginia Tech in 1996. In 1996, he joined the Fiber and Electro-Optics Research Center at Virginia Tech as a Graduate Research Assistant. He earned his Master of Science degree in Electrical Engineering from Virginia Tech in February 1998. Thomas Wavering is currently employed at F&S Inc. in Blacksburg, VA continuing research begun in this thesis.